THE MAGNETITE-RICH BRECCIA MASSES AT IRON MOUNTAIN, SILVER LAKE DISTRICT, SAN BERNARDINO COUNTY, CALIFORNIA

Thesis by

Robert D. Forester

In Partial Fulfillment of the Requirements

for the Degree of

Doctor of Philosophy

California Institute of Technology

Pasadena, California

1953

ABSTRACT

A survey of the vertical magnetic field of the earth was made with an Askania magnetometer at Iron Mountain, Silver Lake District, San Bernardino County, California. The readings obtained were used to draw the lines of equal anomalous intensities, or "isogams", on a geologic map of the mountain. The pattern of the isogams over the alluvium is in accord with the southeast elongation and dip of the orebodies exposed on the hills. The anomalies over the alluvium are probably due to sizable orebodies rather than alluvial material rich in magnetite derived from the exposed orebodies, for the anomalies are of large magnitude and their trend seems unrelated to the present drainage pattern. In some places, the anomalies confirm the fact that the exposed orebodies extend far beneath alluvial cover.

Ore samples were analyzed for magnetic properties and composition. Their mean susceptibility is between 0.10 and 0.17 and their remanent magnetism is about 10 times larger than the magnetism induced by the magnetic field of the earth. Polished sections of the ore indicate that it consists mostly of hematite and magnetite in various ratios, the hematite predominating.

Depths to the centers of magnetic concentrations in the alluvium were determined in two different ways: from application of half-peak value rules to isogams, and from

the analysis of data obtained by measuring magnetic intensities atop a platform placed at the centers of anomalies. Both methods gave values of less than several hundred feet for the depths.

Peak anomalies over vertically polarized, surface-contacting ellipsoids of revolution were computed and plotted as function of true susceptibility, and of the ratio of the principal axes of the ellipsoids. The curves obtained indicate that the exposed orebodies are rather flat. This agrees with the large magnitude of the negative anomalies surrounding the orebodies and with data obtained from holes drilled through three of the orebodies by the U. S. Bureau of Mines.

The ratios of the anomalies expected over vertically polarized ellipsoids of revolution at depth to the anomalies expected for the same ellipsoids at the surface were computed and plotted as a function of the ratio of the principal axes of the ellipsoids. The curves obtained were used to estimate minimum and maximum amounts of ore which could produce the anomalies observed over the alluvium.

Iron Mountain probably consists of two layers of breccia alternating with two layers of conglomeratic sandstone. The ore is confined to the lower layer of breccia. The intensity of deformation and faulting increases westward toward the crystalline-complex. The breccias and conglomeratic sandstone appear to be arched by the uplift of the crystalline-complex.

Four faults trend northeastward. One of the faults offsets a large orebody.

The exposed ore represents erosion remnants capping small hills and ridges. Upon the basis of the magnetic data, the inferred ore beneath alluvial cover was calculated as equal to about 10,000,000 long tons.

The source and structural history of the ores are presented upon the basis of combined geologic, magnetic, and drill-hole data.

ACKNOWLEDGMENTS

The writer wishes to express his gratitude to Dr. Richard H. Jahns for proposing that a magnetic survey be made at Iron Mountain. The writer received inspiration and guidance from Dr. Jahns, who supervised the geological aspects of this survey, and from Dr. Gennady W. Potapenko, who supervised the geophysical aspects of this survey. Dr. Potapenko spent much time critically reviewing the interpretation of the magnetic data.

The writer is grateful to Dr. S. J. Barnett for the use of some of his laboratory equipment in the calibration of the magnetometer and in the determination of the magnetic susceptibility of iron ore samples.

Credit is given to Dr. James Noble and Mr. Lee Silver for the interpretation of the polished sections of the iron ore.

Mr. Richard Sharp was of considerable assistance in obtaining the platform readings.

The wife of the writer performed much of the plane tabling and recording of field data.

CONTENTS

Magnetic anomaly map and structural cross sections are on the back cover.

INTRODUCTION

Iron Mountain is in secs. 11, 12, 13, and 14, T. 15 N., R. 6 E., San Bernardino County, California, and is about 18 miles northwest from the town of Baker. A rough road extends 12 miles eastward from Iron Mountain to U. S. Highway 127, which passes through Baker 8 miles to the south. The nearest railroad is at Baxter siding about 20 miles southwest from Baker. The siding is separated from U. S. Highway 91 by 6 miles of graded road. (See fig. 1.)

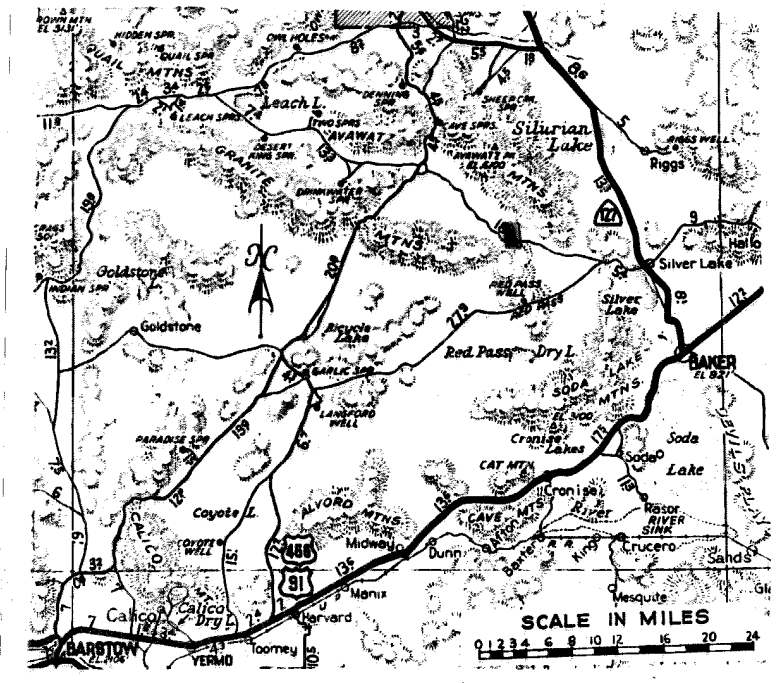

Figure 1. (Location of Iron Mountain shown in red.)

Figure 2. The dark area in the central foreground is Iron Mountain, which is about a mile in length. Talus extending downslope from the orebodies is noted by its streaked appearance.

(Reproduced from Pacific Air Industries photograph.)

The Iron Mountain orebodies consist of long tabular masses of hematite-magnetite that dip, in general, to the southeast. The ore exposed on the hills can be easily shovelled from the surface. The ore which is inferred to lie beneath alluvial cover would have to be mined by open-pit methods.

The mean elevation of the orebodies is about 2400 feet above sealevel. To the north, the Avawatz Mountains rise 3000 to 5000 feet above Iron Mountain. To the south and southwest, smaller mountains, which are an extension of the Avawatz Mountains, rise 1500 feet above Iron Mountain.

The nearest water can be obtained from wells near Silver Lake, which is 12 miles to the east of and 1500 feet below Iron Mountain.

Brief descriptions of the ore deposits at Iron Mountain have appeared frequently in mining journals since 1906. However, a detailed account of its geology and an accurate estimate of its exposed ore reserves did not appear until a joint article by Lamey and Gilluly (1) was published in 1948. Under the auspices of the U. S. Geological Survey, Lamey mapped Iron Mountain in 1943 on a scale of 1000 feet to the inch, and Gilluly remapped Iron Mountain in 1944 on a scale of 200 feet to the inch. Core logs recorded by Gilluly from U. S. Bureau of Mines diamond-drill holes furnished a basis for several cross sections from which tonnage estimates were made. The geology shown on the enclosed anomaly map was compiled partly from the map of

Lamey and mostly from the map of Gilluly. The lithology shown on the anomaly map is reproduced almost entirely from the maps of Lamey and Gilluly; whereas, the fault system is drawn primarily from evidence noted by the writer and does not necessarily coincide with the faults shown by Lamey and Gilluly.

The iron ore breccia lies within the basal portion of a layer of limestone breccia. Associated with the iron ore breccia are separate lenses of quartz monzonite breccia, and lesser amounts of andesite, basalt, and rhyolite breccias. The ore-bearing breccias overlie Tertiary conglomeratic sandstone, possibly with minor angular discordance.

As shown on the anomaly map, limestone breccia caps hills α, β, and γ. It is underlain by Tertiary conglomeratic sandstone and is probably distinct from and stratigraphically above the ore-bearing breccias. Lamey and Gilluly have indicated a single sheet of breccia on their maps, for Gilluly considers the breccias to have been thrust-faulted over the sediments.

Lamey and Gilluly state that the breccias have been derived from a zone of contact-metamorphic minerals associated with a quartz monzonite intrusion. Since the source rocks of the breccias have not been located, it is not possible to tell how far they have been transported. Whether the breccias are sedimentary or tectonic in origin, or both, is a problem not completely solved.

The gangue minerals consist chiefly of limestone and dolomite, and consist of lesser amounts of orthoclase, quartz, and gypsum. Much of the ore is nearly free of gangue, but that which appears conglomeratic or represents zones of partial replacement in limestone may contain from 10 to 50 percent limestone.

The older crystalline rocks west of Iron Mountain, hereinafter designated the "crystalline-complex", consist predominately of quartz monzonite, having phenocrysts of pink orthoclase as much as an inch in length in a grounamass of quartz, biotite, orthoclase, and plagioclase. Locally, the groundmass is rhyolitic. There are lesser amounts of hornblende andesite, diorite, and amygdaloidal basalts.

Although the local dip differs widely in magnitude and direction, the prevailing dip ranges from 10° to 50° to the southeast. The prevailing dip and intensity of folding increase westward toward the crystalline-complex.

Lithology governs the topography. Iron ore and limestone breccias form resistant cappings to ridges and hills that rise several hundred feet above alluvium filled basins. Sandstone crops out in saddles and gullies. Talus and alluvium obscure many of the lithologic contacts. Samples pits reveal the presence of conglomeratic sandstone beneath the ore-bearing breccias. This sandstone is generally stained a reddish-brown as a result of the iron minerals leached from the ore above.

FIELD METHODS

The vertical anomalies at Iron Mountain range between -0.30 and +0.32 oersteds. The fiducial value chosen for the anomalies is equal to the regional (normal), vertical field of the earth, namely, 0.44 oersteds. Hence, the anomalies amount to as much as $\frac{3}{4}$ of the normal, vertical field of the earth. The magnitude of these anomalies obviates some of the refined corrections necessary for most magnetic surveys. The corrections for the diurnal variation of the earth's field, for the effects of temperature on the magnetometer, and for the permanent changes of the elements of the magnetometer produced by shock and wear were lumped into one correction. This was done by distributing the difference between two hourly base checks uniformly among the station occupied in the intervening time. The difference in base checks taken two hours apart varied from 0 to 60 gammas*, and averaged about 25 gammas. Because of the enormousness of the anomalies over outcropping ore, the base corrections for traverses over the exposed orebodies were more a matter of formality than of necessity; and for this reason, four hours were sometimes allowed to elapse between base checks.

The corrections were due largely to effects of temperature on the magnetometer. The magnetic readings decreased rapidly with the rise of the sun on cold mornings, the temperature increasing in an hour from about 4°C. to 15°C. Since a decrease in reading with an increase of temperature required a positive correction, the instrument was under-

*A "gamma" is defined as 10^{-5} oersteds.

compensated for temperature effects. The shift in readings due to the rise in temperature was considerably reduced by "warming-up" the magnetometer in the morning. This was done by opening the door of the magnetometer cover and letting the rising sun shine directly upon the main magnets before taking any readings. In this way, the hourly corrections for the early morning were reduced from about 75 to 25 gammas. During the late afternoon, the corrections became negative as a result of decreasing temperature; however, these corrections were not large, for the temperature decreased slowly. In regions of high magnetic anomalies, any systematically calculated temperature correction is difficult to make, for (according to Heiland (2)) the temperature correction is a function of the vertical magnetic field intensity.

The effects of diurnal variations in the earth's field were small in comparison to the effects of temperature. Throughout the field season, the possibility of magnetic storms was not considered likely, because the agreement between successive base checks was always rather close.

The zero point of the magnetometer decreased some 500 gammas from the first time the instrument was brought into the field in November 1950 until the last time in May 1951. The decrease is too large to be ascribed solely to secular variation of the earth's magnetic field; and hence, may have resulted from one or more of the following: a horizontal shift of the center of gravity of the moving system, a progressive dulling of the quartz knife edges, or a weakening of the main magnets. Since, during the

field season, the sensitivity of the instrument decreased about 1 percent, it is probable that there was either some dulling of the knife edges or weakening of the main magnets, or both, for the sensitivity is inversely proportional to the vertical component of the distance of the center of gravity of the moving system from the knife edges, and directly proportional to the moment of the main magnets. Although the knife edges were visibly chipped, it was possible to duplicate readings to within 5 gammas if the instrument was set up twice in rapid succession at the same location.

The anomalies over the gently sloping alluvium were much lower in magnitude, broader in areal extent, and showed more continuity than those over the ridges and hills outcropping with iron ore. A square network of readings about 100 feet apart was taken over the alluvium; whereas, linear profiles with readings about 50 feet apart were taken in several directions over each of the larger, exposed orebodies. A complete network of readings taken 50 feet apart over the orebodies would be useful, but there was not sufficient time to take the thousands of readings such a close network would have necessitated. On the alluvium, control points were determined by stadia rods. On the ore-bearing hills, stadia rods were used sparingly; rather, mine adits, drill-hole sites, and prominent topographic features were used as control points, because they are accurately located on Gilluly's map, a tracing of which was used to plot the location of the magnetic readings.

Wherever the anomalies changed abruptly, the readings were spaced as close as 25 feet in order that the magnetic profiles might show better continuity and more accurately indicate the true maxima and minima.

In order to obtain additional data for the determination of the depth to the disturbing masses, a platform 11.7 feet high was constructed. It was assembled with brass bolts, wingnuts, and screws in order to be non-magnetic and easily disassembled for automobile transport. However, the platform was not used much for there were only a few places where the anomaly associated with one localized magnetic mass was relatively undisturbed by the influence of a neighboring mass and where the topography was not too steep for a platform setup.

CALIBRATION OF THE MAGNETOMETER

For the calibration of the magnetometer, a coil of 10,000 turns was centered axially over it, so that the quartz knife edges of the magnetometer lay in the plane of the coil. The current which was passed through the coil by dry cells was measured by a precision Weston D. C. ammeter accurate to $\frac{1}{4}$ of 1 percent at full scale after proper temperature correction.

The axial field intensity at the center of the coil is

$$3.1 \qquad H = \frac{2\pi NI}{10R} = 27.05\ I$$

where N= number of turns = 10,000
I= current in amperes through the coil
R= mean radius of the coil = 23.23±0.05 cm

Equation 3.1 considers the coil to be a flat plane of no thickness. To compute the effect due to the thickness, a formula was developed as follows: The equation for field intensity along the axis of a single loop is

$$3.2 \qquad h = \frac{2\pi IR^2}{10(R^2+z^2)^{3/2}}$$

where the new quantity z = the axial distance from the center of the loop

The field intensity at the geometrical center of a coil of many turns may be obtained by integration of equation 3.2:

$$3.3 \qquad H' = \int_{-T/2}^{+T/2} \frac{2\pi NIR^2 dz}{10T(R^2+z^2)^{3/2}} = \frac{2\pi NI}{10\sqrt{R^2+(T/2)^2}}$$

where the new quantity T = the thickness of the coil

The proportional difference between the field intensity determined by the equation 3.1 and that determined by equation

3.3 is

$$3.4 \qquad \frac{H - H'}{H} = \frac{\frac{2\pi NI}{10R} - \frac{2\pi NI}{10\sqrt{R^2 + T^2/4}}}{\frac{2\pi NI}{10R}}$$

$$= \sqrt{1 + T^2/4R} - 1$$

$$\approx 1/8(T/R)^2 \qquad \text{since } 1 >> T/2R$$

For T = 3.75 cm and R = 23.23 cm, equation 3.4 yielded 1/308. Thus the field per unit of current determined by equation 3.1 had to be reduced 1 part in 308 to allow for the thickness of the coil.

A correction was made for the fact that the field intensity acting on the four poles of the paired needles of the magnetometer was greater than the field intensity at the center of the coil. According to Smythe (3), the normal component of field intensity at a point off-center in the plane of a loop is

$$3.5 \qquad H'' = \frac{2\pi NI}{10(R + r)} \left| K + \frac{R^2 - r^2}{(R - r)^2} E \right|$$

where the new quantities are

r = radial distance from the center of the loop =4.1 cm, assuming that the poles are at a distance in from the ends of the needles 1/12 of their length. (See Heiland (2).)

K = an elliptic integral of the first kind

$$\int_0^{\pi/2} \frac{d\theta}{\sqrt{1 - 4Rr \sin^2\theta/(R + r)^2}}$$

E = an elliptic integral of the second kind

$$\int_0^{\pi/2} \sqrt{1 - 4Rr \sin^2\theta/(R + r)^2}\, d\theta$$

Substitution of numerical values into equation 3.5 showed that the field intensity was 2.4 percent greater at the poles than at the center of the loop. Equation 3.1, when corrected for the thickness of the loop and the increased field strength at the pole positions, gave

3.6 $$H = (27.61 \pm 0.10)I$$

The scale sensitivity of the magnetometer was determined by noting the amount of current required by the coil to produce a given deflection of the scale. The sensitivity at the center or zero position of the scale was 0.0183 divisions/gamma. The sensitivity increased monotonically from 0.0176 divisions/gamma at the extreme negative scale deflection of -40 divisions to 0.0190 divisions/gamma at the extreme positive scale deflection of +40 divisions. That the sensitivity is a function of the scale deflection arises from the fact that the vertical component, d, of the distance of the center of gravity of the moving system from the knife edges changes with scale displacement. A negative scale deflection, expressing a decrease in intensity of the vertical field, lowers the center of gravity; and conversely, a positive deflection, expressing an increase in intensity, raises it. Since the sensitivity is inversely proportional to d, the sensitivity would be expected to decrease with a negative deflection, and to rise with a positive deflection. This agrees with the experimental observation.

Since the sensitivity varies with displacement, and since,

it is the tangent of the angle of scale rotation rather than scale displacement which is proportional to changes in the vertical magnetic field, the attempt was made in gathering the field data to keep the scale deflections close to zero by use of the auxiliary magnets.

The auxiliary magnets were calibrated by using the magnetometer as a null device; that is, a scale reading with no magnet and no coil current was recorded. Then, after setting an auxiliary magnet at a known distance from the knife edges, indicated by a brass scale built on the instrument for that purpose, the amount of current required to return the scale to its initial position was then recorded. Current values corresponding to various distances of each of the three magnets from the knife edges were recorded in positions both aiding and opposing the vertical field of the earth, designated respectively, as the S/N and N/S positions. The current values were then reduced to gamma values by equation 3.6. In figure 3[†], the absolute values in gammas are plotted against the distance of the center of the auxiliary magnets from the knife edges.

The scale had a range from -2250 to +2100 gammas about its zero. By various combinations of the scale and the auxiliary magnets in different positions, it was possible to read continuously anomalies from -31,500 to +32,000 gammas.

[†]For details concerning the significance of the curves in figure 3, see note 1 in the appendix.

Figure 3.

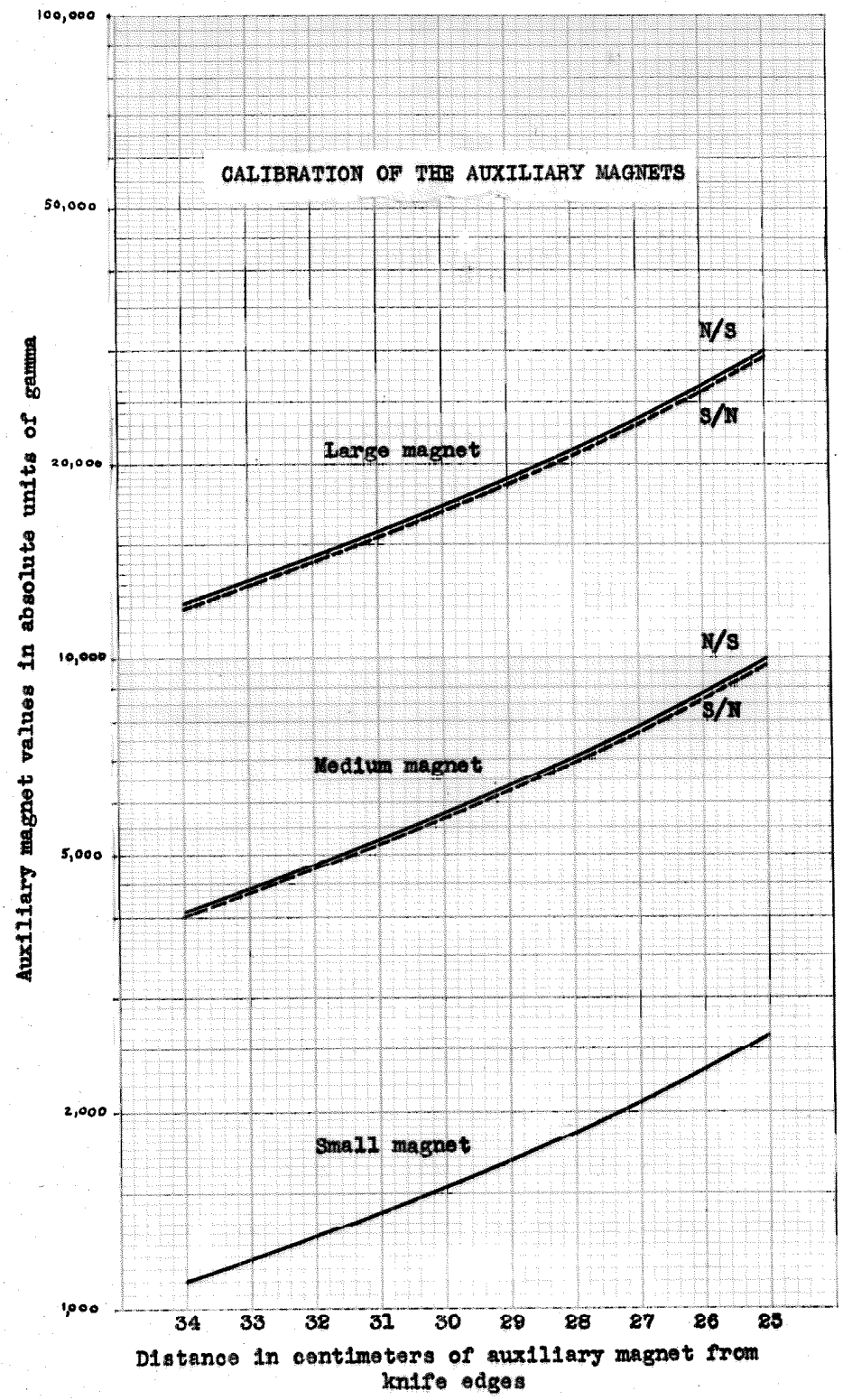
CALIBRATION OF THE AUXILIARY MAGNETS
100,000
50,000
20,000
10,000
5,000
2,000
1,000
Auxiliary magnet values in absolute units of gamma
N/S
S/N
Large magnet
N/S
S/N
Medium magnet
Small magnet
34
33
32
31
30
29
28
27
26
25
Distance in centimeters of auxiliary magnet from knife edges

An attempt to calibrate the magnetometer within a building was abandoned because the field intensity varied erratically, and, as a result of the steel framework of the building, the field intensity was reduced to about half that of its regional value outside. The instrument was calibrated in an open field where the magnetic intensity was comparatively constant as a result of the nearest power lines and buildings being nearly a mile away. At this locality, the vertical field intensity was such that the instrument scale read approximately zero with no auxiliary magnets. This was desirable for no large counter-current had to be sent through the calibrating coil in order to keep the scale near its zero value. Had such a counter-current been necessary, the desired current changes would have been less accurately measured as a result of their superposition upon the counter-current.

An Askania Helmholtz coil†, designed especially for the field determination of scale sensitivity, gave sensitivity values in fair accordance with those given by the single coil. The Helmholtz coil can be used to calibrate the auxiliary magnets. By making the proper interchange of magnets, it is possible to calibrate them in terms of divisions of scale deflection, and after the determination of the scale sensitivity, to reduce them to their effective gamma values. However, this would not be a very accurate procedure, for the scale

† A Helmholtz coil consists of a pair of identical coils oriented so that their axes coincide, and so that the distance between their planes is equal to their diameter.

sensitivity is a function of the deflection. Furthermore, reversed maximum currents through the Helmholtz coil produced a deflection of only 10 scale divisions or about 550 gammas. To calibrate the large magnet, the value of which ranges from 12,000 to 30,000 gammas in its positions of extreme adjustment, in terms of 10 scale divisions equalling about 550 gammas, would be a large extrapolation introducing a compounded error.

Since the single coil had 10,000 turns and the Helmholtz pair had a total of 40, the former required less current to produce a given field intensity than the latter. The use of small currents has the advantage that they can be furnished by dry cells with excellent regulation, and can be measured over a wide range of values on one precision multirange ammeter.

A Helmholtz coil has the advantage over a single coil in that the correction for its axial and radial variation of field intensity is usually negligible. The best type of coil for magnetometer calibration would be a Helmholtz pair with several thousand turns.

ANALYSIS OF ORE SAMPLES

Numerous samples of ore were selected at random from the outcrops of the major orebodies. The orebody from which each sample was taken was recorded.

The streaks of the samples were various shades of black, brown, tan, or red. The streak of an individual sample was rarely a single color. A pure black streak was assumed to be due to magnetite; pure red, to hematite; and tan, to goethite. The streaks showing composite hues were presumed to represent various mixtures of these minerals. Some samples consisted of intergrowths of octahedral, dodecahedral, and even cubic crystals of magnetite as much as an inch in diameter. These crystals had streaks ranging from black to brown, and some of them could be lifted by a permanent magnet. They probably represent primary magnetite (Fe_3O_4) being weathered into martite (Fe_2O_3). No correlation could be made between the streak qualities of the samples and the major orebodies from which they were taken.

Table 1 gives the results of the chemical analyses of the ores listed by Johnson and Ricker (4) of the U. S. Bureau of Mines. The iron content of the four classes of ore analyzed exceeded 52 percent, which is the lowest limit for material acceptable in steel blast furnaces. The high iron content of the deposits is the justification for calling them "orebodies".

Polished sections were made of three ore samples having widely different streak characteristics. Two, or possibly

Analyses of iron ore from Iron Mountain deposits (Silver Lake)

	A	B	C	D
Fe	58.8	57.2	55.6	54.2
Insol.	3.9	2.7		
SiO_2	2.6	1.7	5.9	6.73
S	0.01	0.01	0.13	0.087
P	0.03	0.03	0.014	0.012
CaO	5.6	8.2	4.04	4.49
MgO	2.0	1.2	2.58	2.41
Al_2O_3	0.9	0.8	2.32	2.94
Mn	0.1	0.1	0.05	0.05
Cu	0.06	0.02		
Pb	0.05	0.05		
Zn	Nil	Nil		
TiO_2	0.05	0.05		

A—Surface samples, north outcrop.
B—Surface samples, south outcrop.
C—Ore indicated by diamond drilling.
D—Ore inferred by diamond drilling.

Table 1.

three, primary minerals were noted. The bluish metallic laths were identified as magnetite upon the basis of the black powder produced by drilling into them with a tiny diamond drill. Within these laths were some brighter specks, which might well have been ilmenite, except for the fact that table 1 shows the presence of only a minute amount of titanium. Intergrown with the magnetite were laths of a pitted gray mineral which was the most abundant mineral in the specimens. This mineral was hematite (possibly the specularite form) as evidenced by the bright red powder produced by drilling into it with the diamond drill. The fact that the hematite appeared brighter than the magnetite accords with the larger coefficient of reflectivity commonly listed for hematite. Visual estimates of the mineral content

of the three polished sections are recorded in table 2.

Table 2.

Sample	Magnetite (primary)	Hematite (primary)	Hematite, Goethite, Limestone, and Silicates (secondary)
C253	15%	60%	20%
C254	40	55	5
C255	25	55	20

The fact that C254 jumped readily to a magnet corroborates the visual estimate for it of a high magnetite content.

There is no evidence for the presence of maghemite in the polished sections. According to Newhouse and Glass (5), maghemite is supposed to be developed along fractures, grain boundaries, and along octahedral directions; and it is commonly a weathering product. Diamond drilling into the primary intergrowths of the polished sections failed to disclose any dark brown powder which signifies the presence of maghemite; but some maghemite may have escaped detection in the veinlets filled with soft alteration products. Since, as will be shown subsequently, the magnetic susceptibility of the polished sections seems to be related to the content of magnetite, it is not necessary to postulate the presence of maghemite as the cause of the high susceptibilities. Since the samples which appeared to be almost wholly alteration products had low susceptibilities, little maghemite could be present in the veinlets of secondary minerals.

The high susceptibility of the ore may be attributed entirely to magnetite if the primary hematite in them is of

the ordinary type, the susceptibility of which, according to Heiland (2), ranges from 40×10^{-6} to 100×10^{-6}. Even if the primary hematite should be wholly of the specularite variety, the susceptibility of which, according to Heiland (2), is 3200×10^{-6}, its effect on the susceptibility of ore containing appreciable magnetite would be negligible, for magnetite has a susceptibility several hundred times greater than that of specularite.

By means of the magnetometer, the susceptibilities and the ratios of remanent magnetism to the magnetism induced by the vertical field of the earth were roughly determined for 25 samples. The samples were placed at a known distance beneath the magnetometer and oriented so that both the maximum and the minimum possible readings were obtained. Such readings occurred when the remanent magnetism was oriented essentially parallel to the earth's vertical field, the maximum resulting from the remanent magnetism aiding and the minimum resulting from the remanent magnetism opposing the earth's vertical field. One sample had one minimum and two distinct maxima. The field intensity due to remanent magnetism is

$$4.1 \qquad H_r = \frac{1}{c}\left(\frac{s_1 - s_2}{2}\right)$$

and that due to induction by the vertical field of the earth is

$$4.2 \qquad H_i = \frac{1}{c}\left(\frac{s_1 - s_2}{2} - s_o\right)$$

where c = scale sensitivity
s_1 = maximum scale reading
s_2 = minimum scale reading
s_o = scale reading with sample removed

The ratio of the remanent magnetism to the magnetism induced by the vertical field of the earth is proportional to H_r/H_i. In order to obtain the ratio of the remanent magnetism to the magnetism inducible by the total field of the earth, H_i was multiplied by the ratio of the total field of the earth (0.49 oersteds) to the vertical component of the field of the earth (0.41 oersteds); a step which is justified because the susceptibility of magnetite is nearly constant for small differences in field strength. For 23 out of the 25 samples, the results were conclusive that the ratio of the remanent magnetism to the magnetism induced by the total field of the earth was definitely greater than unity, the median of the ratios being about 10. For the other two samples, the results were indeterminate because they produced no perceptible scale deflection. Since the samples were held at a distance below the magnetometer large compared to their sizes, they were assumed to behave as simple dipoles. The field of a dipole along its axis is

$$4.3 \qquad H_d = \frac{2M}{r^3}$$

where M = the moment of the dipole, or, in this case, the induced moment of the sample
r = the distance between the center of the sample and the main magnets of the magnetometer

Upon substitution of $k'VH$ for M, where k' equals the effective susceptibility, V equals the volume of the sample in cm^3, and H_A the strength of the inducing field in gauss, and

upon solving for k', equation 4.3 becomes

$$4.4 \qquad k' = \frac{r^3 H_d}{2VH}$$

In order to ascertain their true susceptibilities, the demagnetizing effect of the samples upon themselves was considered. Since only rough accuracy was desired, the mean shape of the samples was assumed to be spherical. As a function of the effective susceptibility, the true susceptibility of a sphere is

$$4.5 \qquad k_o = \frac{k'}{1 - 4/3\pi k'}$$

The true susceptibilities calculated by equation 4.5 ranged from imperceptible values to 4.0, and had a median value of about 0.10. The anomalies of the major orebodies could not be correlated with the susceptibilities of the samples taken from them.

In order to determine the susceptibilities of 14 samples accurately, a ballistic method was used. Ballistic methods of susceptibility determinations make use of the fact that the induction current produced in a coil by pulling a magnet through it rapidly is proportional to the moment of the magnet.

In order to eliminate the effects of remanent magnetization, the samples were powdered by means of a mortar and pestle. The powders obtained were put in small cylindrical glass tubes which had corks at both ends. The tubes

averaged about 0.7 cm in diameter in their interiors and 7.0 cm in length. They were jarred to pack the powders as tightly as possible. The density of the powder in each tube was determined to an accuracy of about 1 percent.

The equipment for the accurate determination of the susceptibilities of the powdered specimens comprised a large double-solenoid, and Einstein-de Haas coil[†], a Hibbard Standard flux generator, a test coil, a ballistic galvanometer, batteries, and resistance decade boxes. Figure 4 illustrates how part of this equipment was set up. The Einstein-de Haas coil was centered within the large double-solenoid. The ballistic galvanometer was hooked across the Einstein-de Haas coil. A uniform magnetic field was produced within the large double-solenoid by current supplied by the batteries. The solenoid was oriented at right-angles to the field of the earth in order that the component of the earth's field along the axis of the solenoid would be zero. The specimens whose magnetic

---

[†] An Einstein-de Haas coil consists of a pair of symmetrical double-solenoids placed axially adjacent to each other and wired in opposition so that their combined self-inductance is zero. The deflection produced by moving a magnetic dipole through both solenoids is twice that which would occur for movement through one solenoid. Since this coil enables the specimens to be moved through a uniform field, the effects of eddy currents and of time delay in magnetization are eliminated.

The accuracy of the susceptibility measured by those methods which depend upon the detection of a small change of self-inductance of a coil when the specimen to be tested is placed within it is limited by the necessity of measuring small differences in ballistic swings. When an Einstein-de Haas coil is used, the swing of the ballistic galvanometer is due solely to the magnetic moment of the specimen to be tested.

See note 2 in the appendix regarding the calculation of the coil constant.

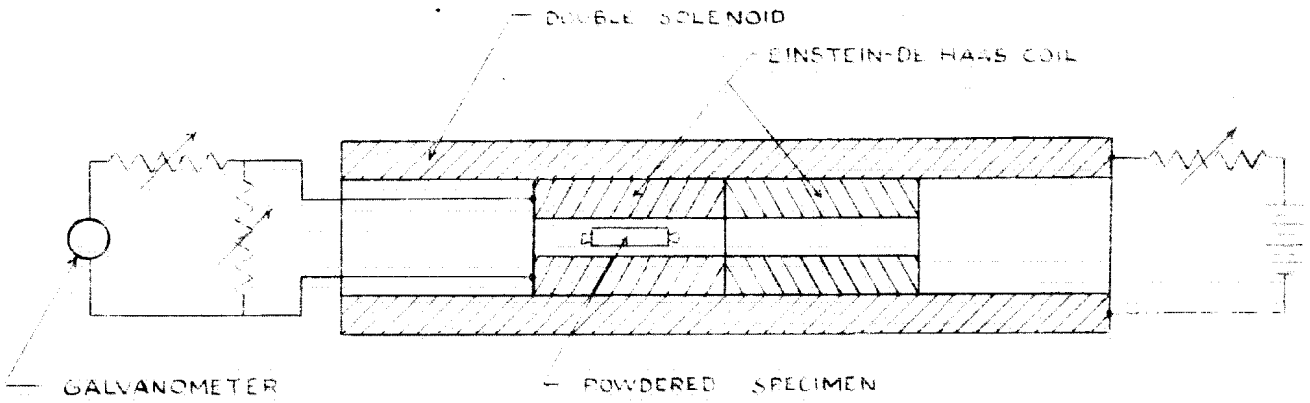

Figure 4. A semi-diagrammatic sketch of part of the equipment used for susceptibility determinations. The double-solenoid and the Einstein-de Haas coil are shown in a longitudinal cross section.

moments were to be determined were jerked from the center of one Einstein-de Haas solenoid to the center of the other, and the resultant deflection on the critically damped galvanometer recorded.

The galvanometer deflection could not be calibrated directly in terms of the accurately known flux generated by the Hibbard Standard, because as a result of the high sensitivity required for the accurate detection of the magnetic moment of the specimens, the lowest flux output of the Hibbard Standard was several times beyond the range of full scale galvanometer deflection. This problem was solved by use of a test coil† which was, in effect, a secondary standard calibrated in terms of the Hibbard Standard.

The galvanometer deflections were non-linear, for the Hibbard Standard did not produce opposite deflections of exactly the same magnitude when the connections to the galvanometer were reversed. However, the correction for non-linearity amounted to an extreme of only 0.25 percent at full scale deflection.

The magnetic moment of a specimen is

$$M = cD \tag{4.6}$$

where c = galvanometer sensitivity determined by use of the intermediary test coil
D = galvanometer deflection due to the specimen

† For details regarding the calibration of the galvanometer, see note 3 in the appendix.

The effective susceptibility of a specimen is

$$4.7 \qquad k' = \frac{M}{VH}$$

where M = magnetic moment of the specimens determined by equation 4.6
V = volume of the powdered specimen
H = magnetic field intensity produced by the large double-solenoid

Substitution into equation 4.7 of IG for H, where I equals the current through the large double-solenoid, and G its coil constant [†], and substitution of cD for M gives

$$4.8 \qquad k' = \frac{cD}{VIG}$$

For a constant magnitude of field in the double-solenoid, each specimen was pulled through the Einstein-de Haas coil four times in the same direction. The polarization in the specimen was reversed for each successive reading. This was done by alternately reversing the field in the double-solenoid and reversing the orientation of the specimen 180°. Owing to the starting of an equilibrium B-H cycle, the first reading was always higher than the last three. Because the galvanometer period was rather short, it was difficult to measure its peak swing precisely; hence, for greater accuracy it was desirable to use the average of the data from several readings. However, only the first reading was valid in determining the initial susceptibility. In

[†] For the calculation of this coil constant, see note 1 in the appendix.

order to improve the accuracy of the determination of the initial susceptibility, a computational procedure using all four readings was developed. The arithmetic mean for each set of four readings was computed. The residual of each first reading from the mean of its set was computed in terms of percentage. Then the mean of the residuals of the first readings for all 14 specimens was computed and found to be 1.1 percent. In order to give a statistically corrected first reading, the mean of each set was increased by 1.1 percent. This correction is based upon the assumption that in a constant magnetizing field, the retentivity of the specimens is linearly proportional to their susceptibility. This entire procedure was performed separately at field strengths of 1, 5, and 25 oersteds, and the effective susceptibilities calculated, respectively, by equation 4.8.

The cylindrical shaped specimens were corrected for magnetometric[†] demagnetization. The true susceptibility, k, in terms of the effective susceptibility, k', and the demagnetizing factor, λ, is

$$4.9 \qquad k = \frac{k'}{1 - \lambda k'}$$

[†]This demagnetization is called magnetometric for it concerns the reduction of the magnetic moment produced by the demagnetizing field, and must not be confused with the reduction of flux through a search coil centered about a straight iron core solenoid, an effect also produced by the demagnetizing field. (See Bozarth and Chapin (6).)

A rigorous solution for the demagnetizing factor of a cylinder oriented with its axis parallel to a uniform magnetic field cannot be developed because the field within the cylinder is not uniform and the susceptibility of ferromagnetic substances is a function of the resultant field strength within them. Because a uniform external magnetic field produces a uniform field within an ellipsoid, a rigorous solution for its demagnetizing factor can be derived. Since the specimens were quite elongated, their shape can be approximated by a prolate ellipsoid of revolution. According to Webster (7), the demagnetizing factor for a prolate ellipsoid of revolution is

$$4.10 \qquad \lambda = \frac{1 - e^2}{e^2}\left|\frac{1}{2e}\ln\left(\frac{1 + e}{1 - e}\right) - 1\right|$$

where $e = \sqrt{a^2 - b^2}/a$ (a is the major axis and b is the minor axis)

The ratio of the diameter to length of the specimens was about 1 to 10. Substitution of $a = 10b$ into equation 4.10 gives 0.020 for λ . This is slightly larger than the true value for the cylinder being approximated, because the mean distance of the divergence of field intensity from the center of the ellipsoid is slightly less than that from the center of the cylinder.

The value 0.020 was substituted for λ into equation 4.9, and the true susceptibilities of the powdered specimens

were calculated. In figure 5 these susceptibilities are plotted as abscissae for field strengths of 1, 5, and 25 oersteds, and the specimens are arranged in order of ascending susceptibility along the ordinate. Straight lines connect the observed points. Because of the inaccuracy resulting from very small galvanometer deflections, the low susceptibility portion of the curve for 1 oersted field intensity was omitted. The observed increase of susceptibility with increasing field strength accords with published results of experiments performed on magnetite at low field strengths. (See Newhouse and Glass (5) and Nettleton and Elkins (8).)

The fact that powdered specimens, AA, C254, and GG had high susceptibilities, had a metallic luster, and were gray-black indicates a high concentration of magnetite. The fact that the other specimens had relatively low susceptibilities, had an earthy luster, and ranged from reddish-brown to tan indicates the predominance of hematite and goethite.

After the test for the induced moments in a field of 25 oersteds was completed, the field in the large double-solenoid was reduced to zero and the specimens were tested for remanent magnetism. Only six samples had remanent magnetism large enough to be measured accurately. (See fig. 6.)

In order to obtain an approximation of the susceptibility of the solid rock from which each powdered specimen was derived, the susceptibility of each powdered specimen

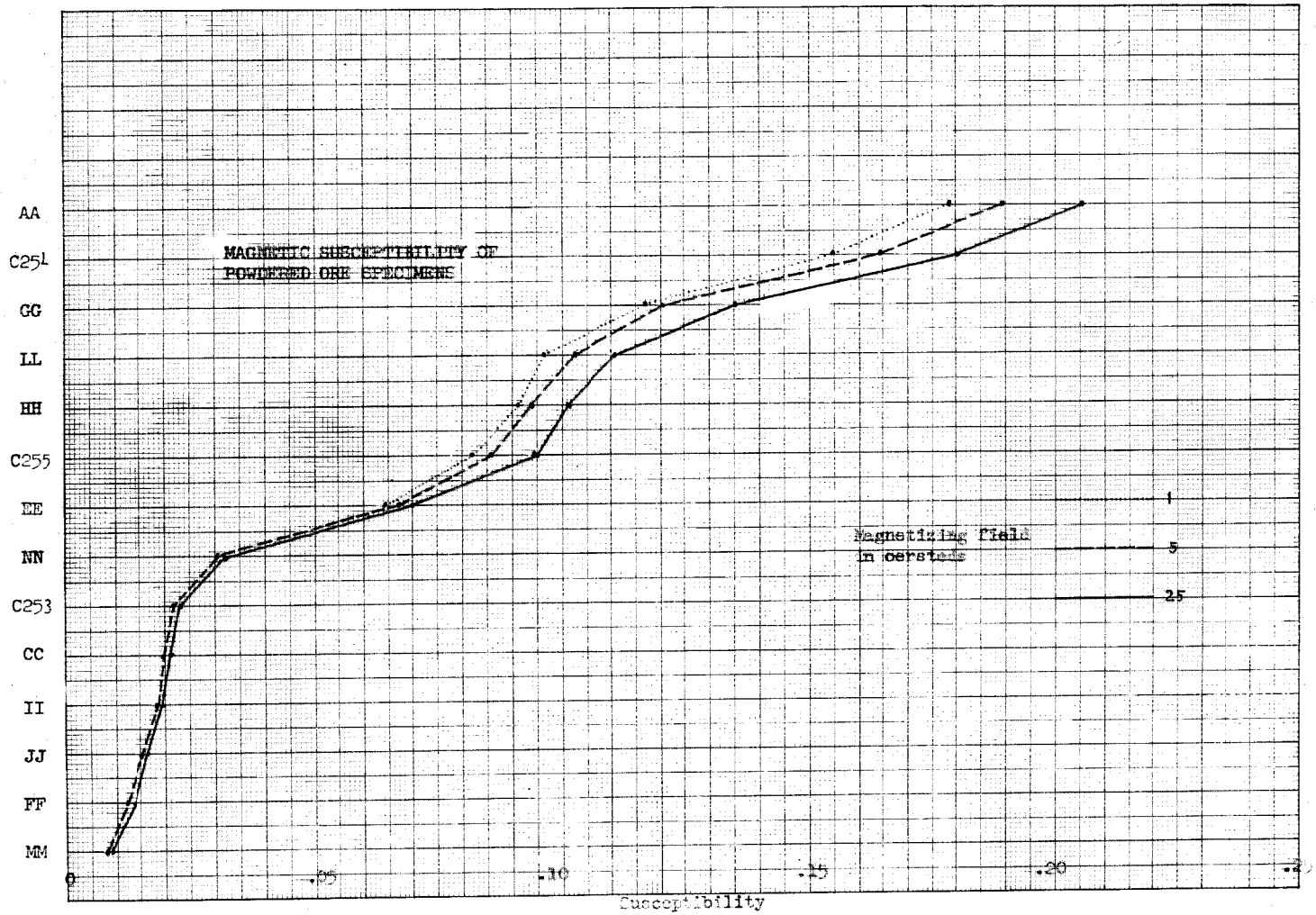
MAGNETIC SUSCEPTIBILITY OF
POWDERED ORE SPECIMENS
AA
C254
GG
LL
HH
C255
EE
NN
C253
CC
II
JJ
FF
MM
Magnetizing field
in oersteds
1
5
25
0
.05
.10
.15
.20
.25
Susceptibility

Figure 5.

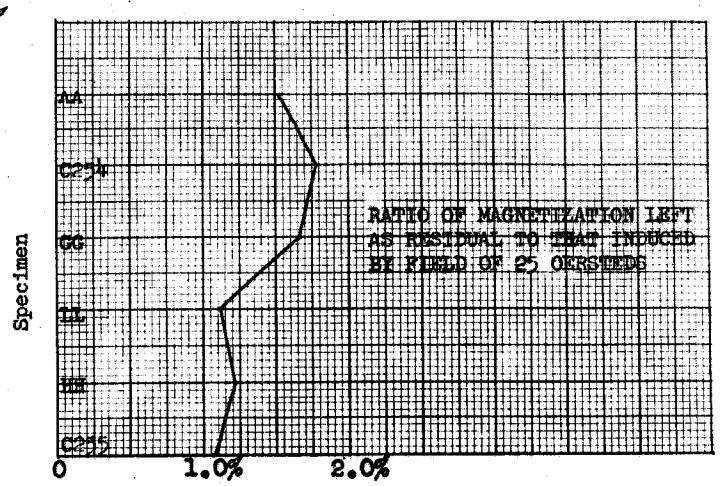

Figure 6.

was multiplied by the corresponding density ratio of the solid to the powder. The results are shown in figure 7. The order of increasing susceptibility is changed somewhat from that in figure 5. The mean susceptibility of the 14 specimens is about 0.10. The density correction is based upon the assumption that the susceptibility is linearly proportional to the magnetite content. This holds true only for low concentrations of disseminated magnetite. The susceptibility of highly concentrated magnetite increases faster than the first power of the magnetite content. Since the magnetite content of the specimens was rather high, the density correction tended to give a susceptibility for the solid form which was too small.

There are three factors which cause the susceptibility

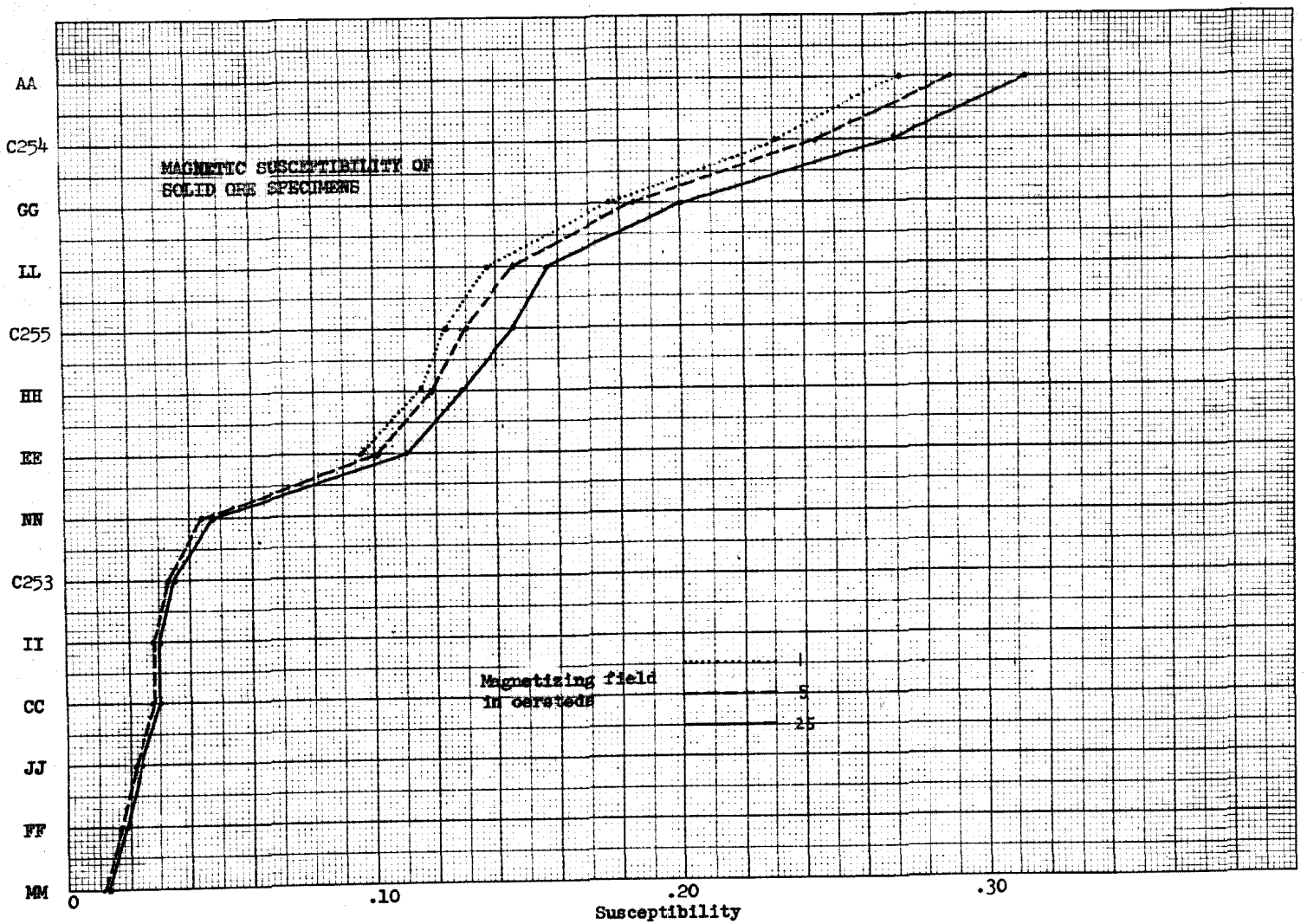
MAGNETIC SUSCEPTIBILITY OF
SOLID ORE SPECIMENS
AA
C254
GG
LL
C255
HH
EE
NN
C253
II
CC
JJ
FF
MM
0
.10
.20
.30
Susceptibility
Magnetizing field
in oersteds
1
5
25

Figure 7.

to increase faster than the first power of the magnetite content:

1. Closer packing tends to eliminate the demagnetization due to the separation of the individual magnetite particles. Maximum limits for this factor can be easily calculated if certain assumptions regarding the shape and distribution of the magnetite particles are made.

2. Owing to the reduction of demagnetization produced by closer packing, the field strength within the magnetite particles is increased. An increase of field strength produces an increase of susceptibility. (See fig. 5.) This factor can be ignored because the change of field strength would not be of large magnitude.

3. Even if the demagnetization is assumed constant, the effective susceptibility of a medium containing a random distribution of magnetite particles is a non-linear function of the magnetite content. The permeability of the magnetite particles was about 2 or 3, and that of the interstitial material consisting of air, hematite, and gangue minerals was about 1. Because of the relatively small permeability contrast within the specimens, the departure of the susceptibility from a linear dependence upon the magnetite content was not overly large. Although this factor is significant, it has been ignored because it is difficult to compute.

The effect of only the first factor was calculated. An upper limit for the susceptibility of the solid specimens

was made on the assumption that the magnetite existed as isolated spheres in the powdered form and that it pervaded the solid form homogeneously. The mean susceptibility of the solid samples, 0.10, was substituted into equation 4.5. This yielded a maximum susceptibility of 0.17. This maximum is probably large enough to account also for the second and third factors. It is of the same order of magnitude as the susceptibility of the solid samples crudely determined by the magnetometer. The actual mean susceptibility of the solid samples is probably between 0.10 and 0.17.

The curves in figures 5 and 7 rise somewhat hyperbolically with increasing susceptibility, and thus indicate that the susceptibilities of the specimens are skewed toward the low values. This probably results both from the fact that the mean volume concentration of magnetite in the ore is much less than 50 percent and from the fact that the susceptibility increases faster than the first power of the magnetite concentration. The two humps on the curves are second order features which might not appear with a larger sampling of the population. The powdered specimens, which were derived from the comminution of cobble-sized ore samples, have a wide range of susceptibility. The spread of susceptibility values might have been considerably reduced had the powdered specimens been derived from ore samples the size of boulders, and, accordingly, the estimate of the mean susceptibility would have been more accurate.

Because susceptibility is not only a function of

magnetite concentration, but also of the shapes of the magnetite particles and their positions relative to each other, an accurate estimate of magnetite concentration cannot be made from the susceptibility alone. For samples having large susceptibilities, the "packing effect" causes the magnetite concentration to be overestimated. Such an overestimate occured when the magnetite concentrations of the powdered specimens corresponding to the polished sections were calculated from their susceptibilities. The concentration of magnetite calculated in this manner for polished section C254 was about twice that estimated for it visually.

Most striking is the result that for a field of 25 oersteds, the magnitude of remanent magnetism (see fig. 6) was only 1 to 1½ percent of the magnitude of the induced magnetism; whereas, the ratio of remanent magnetism to magnetism induced by the earth's field was about 10 to 1 for 23 out of 25 samples. In places, the ore has apparently been exposed to field intensities large enough to produce magnetic saturation. Neither telluric currents nor the indirect inductive action of electrical discharges in the atmosphere would seem to have magnitudes sufficient to produce this large remanent magnetism. The chance that all the samples were picked from the boundaries of the orebodies where the divergence of the magnetization was unusually large does not appear great, for the sampling was conducted randomly, and at least some of the 25 samples would be expected to have remanent magnetism equal to or much below that

ascribable to induction by the field of the earth. Perhaps, this remanent magnetism resulted from the cooling of ore formed at temperatures above the Curie point and at extraordinary pressures. The magnitude of such an effect is, however, unknown. An explanation which readily suggests a cause potent enough for such universally large magnetization is that lightning has struck the orebodies from time to time. According to Heiland (2), currents of 20,000 amperes are common in lightning discharges.

As shown subsequently, the magnitude and distribution of the magnetic anomalies over the orebodies, although locally erratic, are in general accord with induction by the present field of the earth. This implies that the effects of induced magnetism predominate over those of remanent magnetism. Two hypotheses are advanced to explain this discrepancy:

1. During times of electrical disturbance, electrons are attracted by the inductive action of the atmosphere to a thin, upper surface layer of the earth; therefore, the current from the ensuing lightning discharges and, hence, the effects of magnetic induction concomitant with them are most concentrated at the surface. No samples of solid ore were taken at depth to test whether or not the remanent magnetism decreases downward.

2. The source rock from which the orebodies were derived was strongly magnetized by lightning. Although the original polarization might have been unidirectional, the disintegration of the source rock randomly disoriented the polarization;

and as a result, although the remanent magnetism is preserved in the component rocks of an orebody, its mean effect over an entire orebody is approximately nullified.

INTERPRETATION OF THE ANOMALIES

Explanation of the Anomaly Map

At Iron Mountain the regional magnetic field has a vertical intensity of 0.44 oersteds, an inclination of about 60°, and a declination of 15°.7 to the east. The zero level for the anomalies was chosen over the alluvium where they had a minimum range of values. Such places were far from the orebodies and contained little iron ore float. The zero level chosen was 0.015 oersteds higher than the vertical field intensity recorded 12 miles to the east at Silver Lake, which is a playa.

Since Iron Mountain is faulted, in part at least, against the crystalline-complex, and since the exposed crystalline-complex shows a wide regional variation in composition, little inference concerning the composition of the basement beneath Iron Mountain can be made upon the basis of surface geology. However, the negative anomalies over the crystalline-complex increase uniformly toward zero as the distance from the orebodies increases, a fact which may indicate that the basement beneath Iron Mountain is also composed of quartz monzonite. The high degree of continuity of the anomalies over the quartz monzonite attests its homogeneity and tends to exclude the presence of magnetite-rich streaks within it.

The shallow deposits of iron ore and the talus derived therefrom tend to mask the effects of the underlying basement.

The basement probably does not affect the local variation of anomalies at Iron Mountain, but may significantly affect the regional variation, and thus influence the value chosen for the zero level.

The susceptibility of the conglomeratic sandstone is quite insignificant. The susceptibility of the limestone is probably insignificant in spite of the fact that iron minerals transect it locally. Wherever the alluvium is rich in iron ore talus, large susceptibilities exist.

Isogams (isanomaly contours) were drawn over the alluvium and crystalline-complex, which are places where the readings showed definite continuity from station to station. On the hills where the orebodies outcrop, there was little continuity even with 25 foot spacing between readings; therefore, contouring over the exposed orebodies is unwarranted.

With little loss of accuracy in the placement of isogams, the anomalies were expressed to the nearest 100 gammas. The isogam interval was selected as 500 gammas up to anomalies of $|2000|$ gammas, and as 1000 gammas for anomalies above $|2000|$ gammas. Isogams were not drawn for values greater than $|4000|$ gammas, because such values exist in the immediate vicinity of the orebodies and thus show little continuity.

Apparently, there is no broad regional anomaly embracing the whole of Iron Mountain. This is indicated by the fact

that, even in places of intense anomalies, the zero isogam demarks the limit between closed positive and negative isogams. Furthermore, separate areal integration of the recorded positive and negative anomalies would give approximately equal values. The intensity of the localized anomalies over Iron Mountain renders the detection of a regional anomaly difficult. For this reason a second derivative map of the area was not made. In order to detect the regional anomaly accurately, a broad strip of readings several times the area previously covered should be taken entirely around Iron Mountain, a strip which would be characterized by much less local variation of the anomalies.

The calculation of a second derivative map of the alluvium, in order to leave as residual, second order features associated with its closed isogams, could not be made easily, for the lack of uniform spacing among the stations requires laborious interpolation among station values; nor accurately, for the distance between stations is a sizable fraction of the first order features indicated by the closed isogams.

Attempts to make exact determinations of the depth, form, and magnitude of the orebodies are difficult because the proximity of the orebodies to each other affords poor resolution of their respective anomalies, and because the effects due to remanent magnetization are rather significant. The qualitative interpretation of the anomalies should be stressed over a quantitative one. Calculations are made in order to ascertain relative magnitudes rather than precise values.

The shallow disturbing masses tend to mask the effects of the deep ones. In two definite instances, rather large anomalies were associated with a superficial thickness of iron-rich talus. The zero contour between positive anomaly Λ and negative anomaly θ coincides with the termination of the iron-rich talus eroded from orebody C. The high positive anomalies on the bank of the gully due south from orebody C exist over mounds of iron-rich talus which are as much as ten feet thick.

The effects of remanent magnetization, although strong, are rather localized, for the anomalies over the orebodies generally accord with induction by the present field of the earth. Even though the susceptibilities determined for the surface ore samples had a wide range of values, it is possible that the mean susceptibility of a large number of samples would be fairly constant, and would approximate the mean susceptibility within the interiors of the orebodies. This assumes that the orebodies are essentially homogeneous on a large scale. Locally, however, the orebodies appeared unevenly weathered, and showed variable composition. Some ore was massive and nearly pure while other ore appeared conglomeratic in nature and contained considerable limestone gangue.

Analysis of the Exposed Orebodies

Since negative extreme anomalies of a magnitude equal to about a fifth that of the central positive extreme anomaly surrounds most of the exposed orebodies, and since these negative extremes tend to be compressed close to the boundaries of the orebodies, the orebodies cannot extend to great depth. A magnetic mass which extends deep within the earth tends to be unipolar, its positive anomalies extending far beyond the surface projection of its periphery, and its encircling negative anomalies having low magnitude and large areal spread.

If only the vertical component of the earth's field is considered, the ratio of the outer negative extreme to the central positive extreme is exactly 1/54 around a sphere and 1/8 along the two sides of an infinite horizontal cylinder. If the earth's total field is considered, these ratios are not constant about a sphere nor along the two sides of an infinite horizontal cylinder, but the northern negative extreme is considerably larger than the southern negative extreme. However, the mean value of the negative extremes taken around either figure is approximately the same as the constant value due to the vertical component of the earth's field alone. For an inducing magnetic field inclined at 60°, the ratio of the northern negative extreme to the central positive extreme is about 1/13 for a sphere and about 1/3

for an infinite horizontal cylinder oriented perpendicular to the magnetic meridian; and the ratio of the southern negative extreme to the central positive extreme is about 1/300 for a sphere and 1/24 for the cylinder. For an infinite horizontal cylinder oriented parallel to the magnetic meridian, the anomalies are independent of the horizontal component of magnetization; consequently, the ratio of the negative extreme to the positive extreme is 1/8, the value due to the vertical component alone.

If the information in the last paragraph is used as a criterion, the fact that the magnitudes of the negative extremes are actually equal to about a fifth that of the positive extremes indicates that most of the orebodies must be flatter than either a sphere or an infinite horizontal cylinder. Allowance must be made wherever compared extremes do not lie nearly in a horizontal plane.

It is difficult to tell whether or not the presence of abrupt negative anomalies within the surface boundary of an orebody is the result of a local decrease in magnetite concentration, the effects of remanent magnetization, a thinning of the orebody, or a descent toward the negative pole of the orebody. Some of the marked decrease in the positive anomalies away from the epicenters of the orebodies probably results from the thinning of the orebodies towards their peripheries.

Locally, the anomalies over some orebodies appear

chaotic. This is especially true over orebodies D, E, and J. In places, the compass needle was rotated 90° or even reversed from the direction of the regional magnetic north. Such effects probably attest the strong localized influence of remanent magnetism. The peaks of orebodies E, J, and H have negative anomalies and the peak of orebody D has a small positive anomaly. The absence of large positive anomalies at these peaks may have resulted from strokes of lightning. As a result of the erratic anomalies over the orebodies, the effects of the inductive action of the earth's horizontal field are obscured. There is no clear evidence that the horizontal field has appreciably shifted, as expected, either the positive extremes to the magnetic south or the negative extremes to the magnetic north.

Deep magnetic disturbances are commonly analyzed by assuming them to be spheres, infinite horizontal cylinders of revolution, or slabs extending to infinity in one or two dimensions. This is justifiable because the detectability of higher order features decreases as the depth to the disturbing body increases. Thus, for an irregular equidimensional body, the magnetic contours become increasingly circular; and for an irregular body very long in one horizontal direction, the magnetic contours approach straight lines parallel to the elongate axis of the body.

The simple figures used to analyze a deep body are not suitable for a shallow body, especially one which contacts

the surface. Although the analysis of a shallow body is more complicated than that for a deep one, the shape and extent of a shallow body can be defined within smaller limits. However, the magnetic contours over a shallow body are influenced much more by its upper surface than by its lower surface.

Since the shape of an orebody can commonly be approximated by a triaxial ellipsoid, elaborate tables giving the magnetic contours over ellipsoids of various shapes, sizes, depths, and directions of polarization would be useful for the analysis of a shallow orebody. Since the computations for a complete set of tables would be too laborious, the number of variables were reduced and four simple graphs were constructed.

As an aid in the analysis of the orebodies exposed on the hills, two graphs (figs. 8 and 9) were plotted giving the anomaly at the peak of uniformly, vertically polarized ellipsoids of revolution. Both graphs consist of a family of curves in which the abscissa represents the true susceptibility of the body; and the ordinate, the anomaly in gammas. The ratio of the axis of revolution, a, to the transverse axis, b, is a parameter for the curves. Figure 8 gives the anomaly at the tip of the axis of revolution for ellipsoids with vertical axes of revolution, as computed from equation 5.1a, for oblate ellipsoids, and from equation 5.1b, for prolate ellipsoids. Figure 9 gives the anomaly at the tip of the vertical transverse axis for

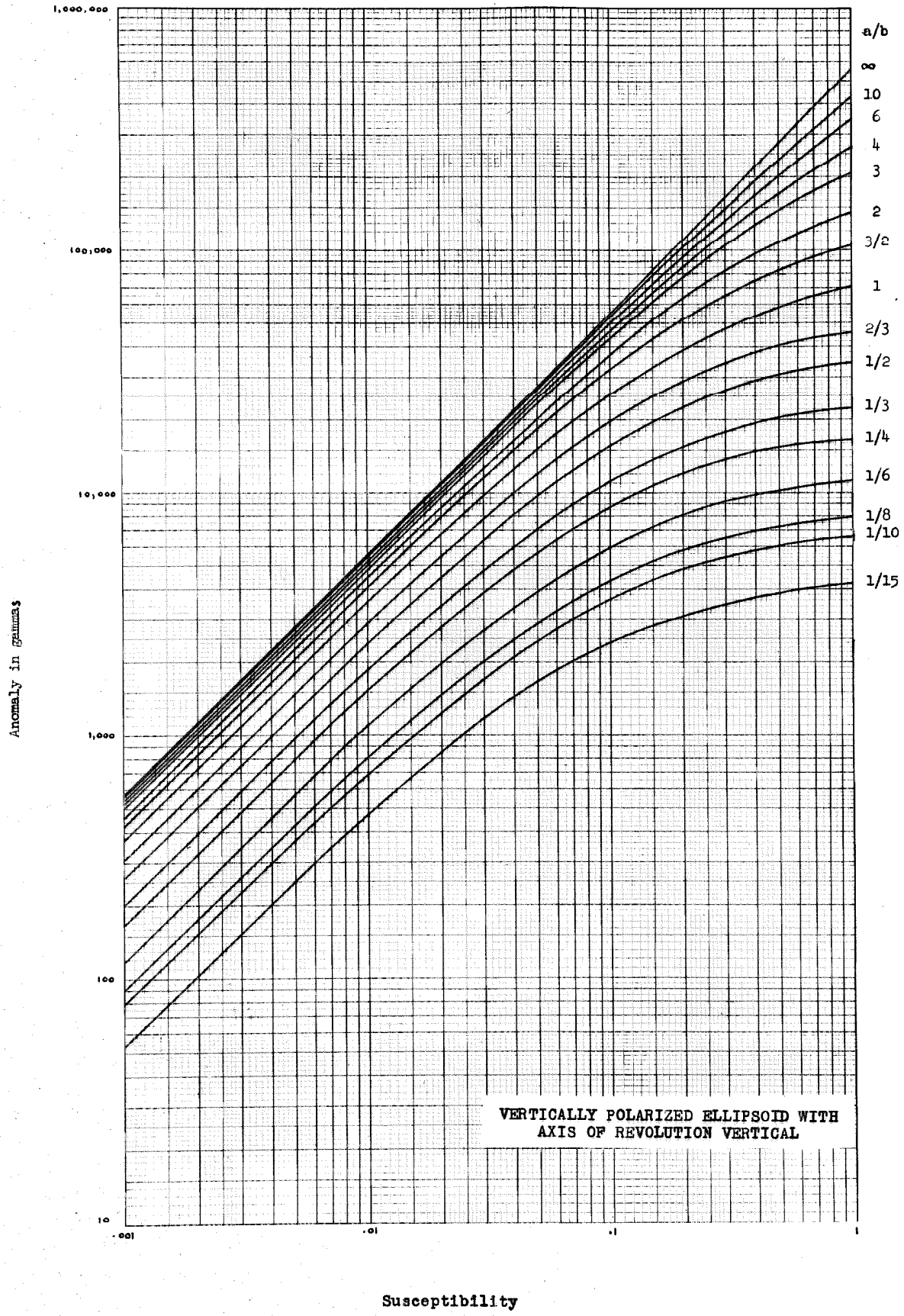
1,000,000
100,000
10,000
1,000
100
10
.001
.01
.1
1
Anomaly in gammas
Susceptibility
a/b
∞
10
6
4
3
2
3/2
1
2/3
1/2
1/3
1/4
1/6
1/8
1/10
1/15
VERTICALLY POLARIZED ELLIPSOID WITH
AXIS OF REVOLUTION VERTICAL

Figure 8.

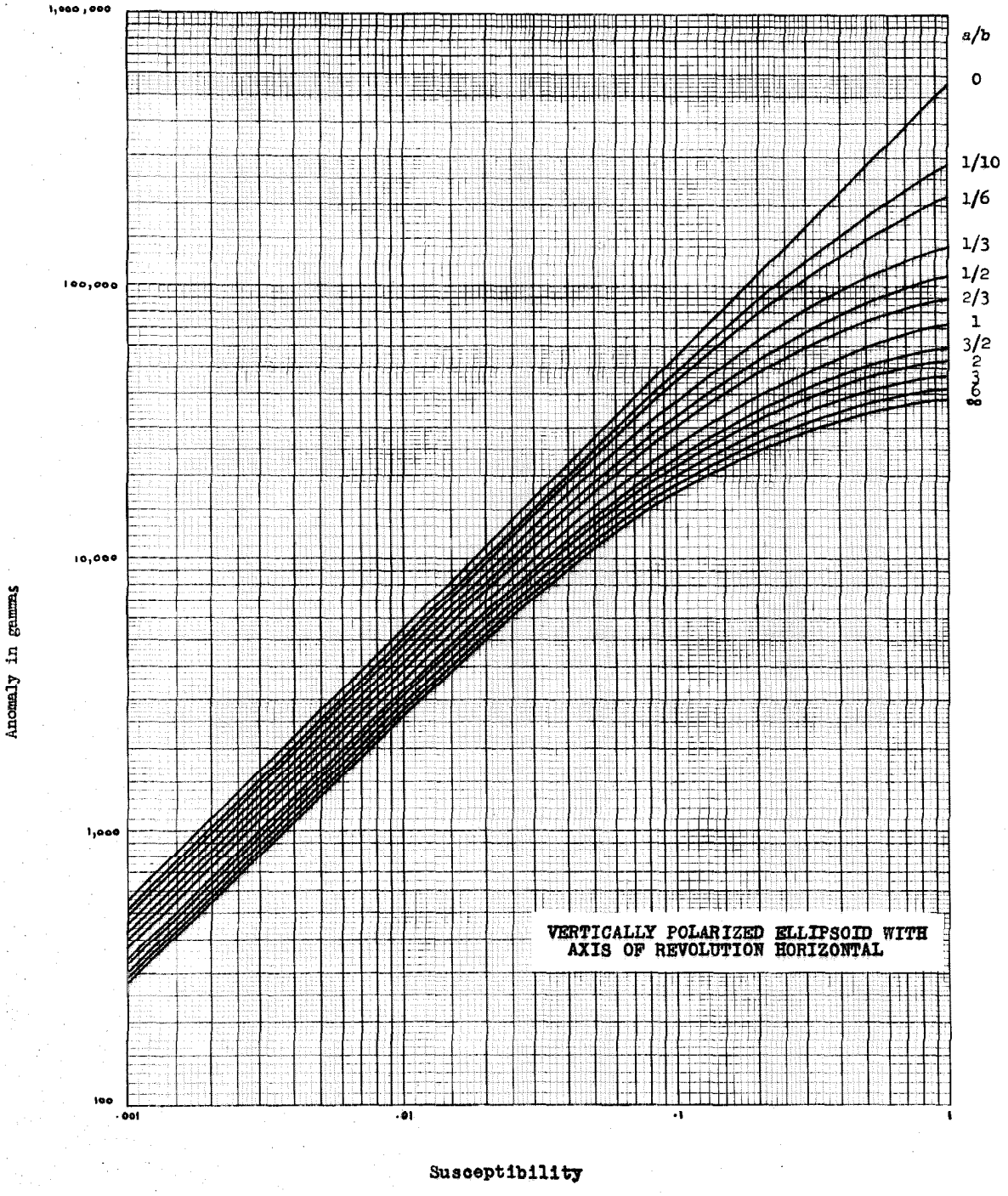
1,000,000
100,000
10,000
1,000
100
Anomaly in gammas
.001
.01
.1
1
Susceptibility
a/b
0
1/10
1/6
1/3
1/2
2/3
1
3/2
2
3
6
∞
VERTICALLY POLARIZED ELLIPSOID WITH
AXIS OF REVOLUTION HORIZONTAL

Figure 9.

ellipsoids with horizontal axes of revolution, as computed from equation 5.2a, for oblate ellipsoids, and from equation 5.2b, for prolate ellipsoids. These equations were derived from more elaborate equations given by Koenigsberger (10).

5.1a $$\Delta Z = \frac{4\pi Zk}{1+\lambda k}\left[1 - \frac{ab^2}{(b^2-a^2)^{3/2}}\left(\frac{\sqrt{b^2-a^2}}{a} - \operatorname{arctg}\frac{\sqrt{b^2-a^2}}{a}\right)\right]$$

5.1b $$\Delta Z = \frac{4\pi Zk}{1+\lambda k}\left[1 - \frac{ab^2}{(a^2-b^2)^{3/2}}\left(\ln\left|\frac{a+\sqrt{a^2-b^2}}{b}\right| - \frac{\sqrt{a^2-b^2}}{a}\right)\right]$$

5.2a $$\Delta Z = \frac{4\pi Zk}{1+\lambda k}\left[1 - \frac{ab^2}{2(b^2-a^2)^{3/2}}\left(\operatorname{arctg}\frac{\sqrt{b^2-a^2}}{a} - \frac{a\sqrt{b^2-a^2}}{b^2}\right)\right]$$

5.2b $$\Delta Z = \frac{4\pi Zk}{1+\lambda k}\left[1 - \frac{ab^2}{2(a^2-b^2)^{3/2}}\left(\frac{a\sqrt{a^2-b^2}}{b^2} - \ln\left|\frac{a+\sqrt{a^2-b^2}}{b}\right|\right)\right]$$

where Z = vertical field intensity (0.44 oersteds at Iron Mountain)
a = length of the axis of revolution, and for equations 5.1a and 5.1b represents the depth to the center of the ellipsoid
b = length of the transverse axes, and for equations 5.2a and 5.2b represents the depth to the center of the ellipsoid
k = true susceptibility, which is assumed as uniform throughout the ellipsoid
λ = demagnetizing factor:

for eq. 5.1a $$\frac{4\pi ab^2}{(b^2-a^2)^{3/2}}\left(\frac{\sqrt{b^2-a^2}}{a} - \operatorname{arctg}\frac{\sqrt{b^2-a^2}}{a}\right)$$

for eq. 5.1b $$\frac{4\pi ab^2}{(a^2-b^2)^{3/2}}\left(\ln\left|\frac{a+\sqrt{a^2-b^2}}{b}\right| - \frac{\sqrt{a^2-b^2}}{a}\right)$$

for eq. 5.2a $$\frac{2\pi ab^2}{(b^2-a^2)^{3/2}}\left(\operatorname{arctg}\frac{\sqrt{b^2-a^2}}{a} - \frac{a\sqrt{b^2-a^2}}{b^2}\right)$$

or eq. 5.2b $$\frac{2\pi ab^2}{(a^2-b^2)^{3/2}}\left(\frac{a\sqrt{a^2-b^2}}{b^2} - \ln\left|\frac{a+\sqrt{a^2-b^2}}{b}\right|\right)$$

In figure 8, the curve for $a/b \rightarrow \infty$ represents the limiting case for a vertical straight line, and the curve for $a/b=1$ represents a sphere. The curve for $a/b=0$ represents the limiting case for a flat plane of no thickness, the anomaly of which approaches zero, and thus cannot be shown on logarithmic coordinates.

In figure 9, the curve for $a/b=0$ represents the limiting case of a vertical plane of no thickness, the curve for $a/b=1$ corresponds identically to the sphere represented in figure 8, and the curve for $a/b \rightarrow \infty$ represents the limiting case of an infinite horizontal cylinder.

The curve in figure 8 for $a/b \rightarrow \infty$ and the curve in figure 9 for $a/b=0$ are straight lines because they represent limiting cases in which the demagnetizing factor is zero, or in other words, the effective susceptibility is equal to the true susceptibility. The deviation of the other curves from a straight line becomes more pronounced as the demagnetizing factor increases. For the case of susceptibility approaching infinity, the curves approach a horizontal asymptote determined by the reciprocal of the demagnetizing factor; $\lim_{k \rightarrow} \frac{k}{1 + \lambda k} = \frac{1}{\lambda}$

The curves in figures 8 and 9 are dependent upon the shape but not the size of the ellipsoids. They give the anomaly at the peaks of various ellipsoids, points where a horizontal plane is tangent to the ellipsoids. Consequently, if the curves are to be applied to the field data, the height of the observations above the surface of the orebodies must be small in comparison to the size of the orebodies.

The contribution of horizontal magnetization to the anomaly at the peaks of the ellipsoids is zero, for these peaks lie on the vertical axes about which the ellipsoids have radial symmetry. If the horizontal magnetization is neglected, the anomaly at the peaks of the ellipsoids is also the positive extreme anomaly. If, however, horizontal magnetization is considered and the readings are confined to the horizontal plane tangent to the ellipsoids, the positive extreme is larger than the anomaly at the peak and is, in general, located slightly south of it. The complexity resulting from horizontal magnetization is bared if one considers that an oblate ellipsoid which is magnetized in the northern hemisphere of the earth and which dips at a small angle to the south has two positive extremes, one south of and the other larger one north of the epicenter of the ellipsoid. (See Koenigsberger (10).)

For a prolate ellipsoid oriented either vertically or horizontally and parallel to the magnetic meridian, the effects of horizontal magnetization are negligible, in fact, they approach zero as the eccentricity increases to the point where the ellipsoid resembles an infinite cylinder of revolution.

The effects of horizontal magnetization are negligible on an oblate ellipsoid with a horizontal axis of revolution; in fact, the effects approach zero as the eccentricity of the cross section parallel to the axis of revolution increases

to the point where the ellipsoid resembles a vertical dike of infinite depth.

In an inducing field inclined at an angle of 60°, a sphere has a positive extreme which is 10.2 percent larger in magnitude than the anomaly at its peak, and an infinite cylinder oriented perpendicular to the magnetic meridian has a positive extreme which is 10.3 percent larger in magnitude than the anomaly along its crestline. Since a prolate ellipsoid changes from a sphere to an infinite cylinder as its eccentricity varies from zero to infinity, it can be concluded that the effects of horizontal magnetization on a prolate ellipsoid oriented perpendicular to the magnetic meridian are significant, but not large.

The anomalies over a sphere depend appreciably upon the horizontal magnetization. The anomalies of a flat slab become due almost wholly to horizontal magnetization as the flat slab decreases in thickness to the point where it resembles a plane. Since an oblate ellipsoid changes from a sphere to an infinite plane as its eccentricity varies from zero to infinity, it can be concluded that the effects of horizontal magnetization on an oblate ellipsoid with a vertical axis of revolution are relatively large.

It can be stated, from the information in the last four paragraphs, that except for oblate ellipsoids with vertical axes of revolution, the effects of horizontal magnetization on the ellipsoids considered in figures 8

and 9 are small, and can be neglected if only the relative magnitudes of the anomalies are of interest. For an orebody being approximated by an oblate ellipsoid with a vertical axis of revolution, the horizontal magnetization can be neglected if care is taken to see that the anomaly for use in figure 8 represents the value at the geometrical epicenter of the orebody rather than the positive extreme, which is generally located slightly south from this epicenter.

Actually, no orebody is either uniformly magnetized or shaped as a perfect ellipsoid. Consequently, the graphs in figures 8 and 9 are a set of comparative norms to be used with discretion. Given any two of the three variables, namely, the susceptibility, the anomaly, or the ratio of the principal axes, the third can be estimated from the graphs. The graphs were applied in the interpretation of orebodies F, F_1, G,and D, and to anomaly Σ. The mean susceptibility of the orebodies was assumed to be between 0.10 and 0.17, which is the interval determined previously for the ore samples.

For a mean central anomaly of 15,000 gammas, orebody F is, according to figure 8, a flattened ellipsoid with $0.47 > a/b > 0.36$. If b is assumed to equal 150 feet, the mean value for the horizontal outcrop radius, the depth to the center of the orebody is between 55 and 75 feet.

For a mean central anomaly of 10,000 gammas, orebody F_1 is, according to figure 8, a flattened ellipsoid with

$0.29 > a/b > 0.22$. For a mean value of b equal to 70 feet, the depth to the center of orebody F_1 is between 15 and 20 feet.

For a mean central anomaly of 10,000 gammas, orebody G is according to figure 8, a flattened ellipsoid with $0.60 > a/b > 0.43$. For a mean value of b equal to 115 feet, the depth to the center of orebody G is between 50 and 70 feet.

The mean central anomaly along the crest of orebody D is about 15,000 gammas. On the basis of diamond-drill information, this orebody resembles an ellipsoid having three axes of unequal length. (See fig. 10.) The longest axis, which dips slightly to the southeast, is about four times the length of the transverse horizontal axis, and about twelve times the length of the transverse vertical axis. The orebody was compared first to an oblate ellipsoid with a vertical axis of revolution and then to a prolate ellipsoid with a horizontal axis of revolution. For an anomaly of 15,000 gammas and for $a/b=1/3$, figure 8 gives a susceptibility of 1.8 for the orebody as approximated by the oblate ellipsoid. For the same anomaly and for $a/b=4$, figure 9 gives a susceptibility of 0.67 for the orebody as approximated by the prolate ellipsoid. Since the actual shape of the orebody is a composite of the prolate and oblate ellipsoids, the true susceptibility should be in the interval between 0.67 and 1.8. Although this overlaps

A

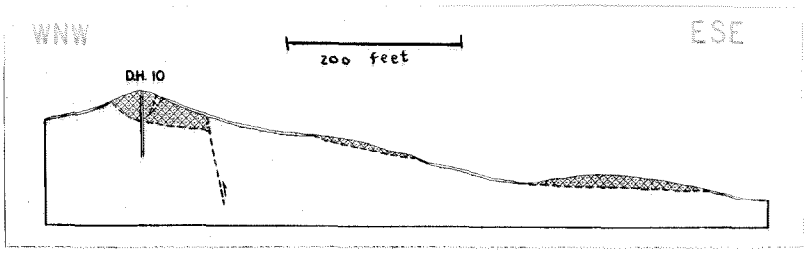

B

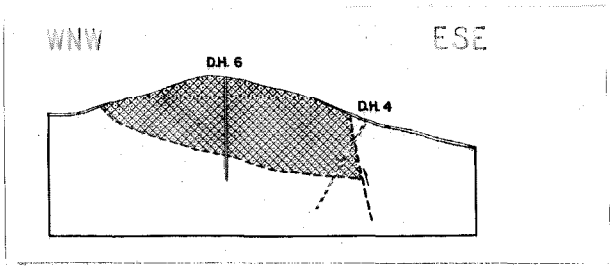

C

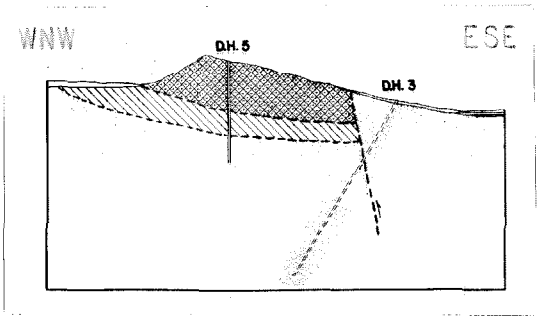

D

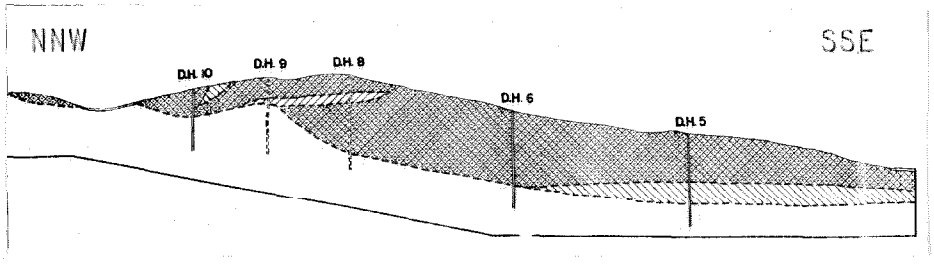

Figure 10. Reproduction of sections through orebody D published by the U. S. Geological Survey:
A. WNW-ESE section through the northern tip.
B. WNW-ESE section through the middle.
C. WNW-ESE section through the lower third.
D. NNW-SSE section through the central part.
(The cross-hatched area represents magnetite breccia; parallel lines dipping to the left, dolomite breccia; and parallel lines dipping to the right, andesite breccia.)

the interval between 1.0 and 1.7 determined for the ore samples, the geometric mean of the interval for orebody D is considerably less than that of interval for the ore samples.

The surface layers of the orebodies have probably been weathered more than the regions deep within the orebodies. Hence, it is possible that as a result of the oxidation of magnetite to martite, the concentration of magnetite in the surface layers is less than that deep within. However, as evidenced by its abundance in clean beach sands, magnetite is one of the most resistant of the accessory rock-forming minerals. Hence, it is also possible that as a result of the leaching of soluble gangue minerals, the surface layers contain a greater concentration of magnetite than the inner regions of the orebodies. Evidence for the latter possibility can be seen from examination of table 1. Table 1 indicates that the surface ore has a slightly greater concentration of iron and CaO and a smaller concentration of the oxides of aluminum, silicon, and magnesium than the ore within the orebodies. This indicates that the soft clay minerals have been carried off by surface water, leaving the iron ore and limestone as residual concentrates. The resemblance of the surface of the orebodies to lag gravels denotes the absence of soft, "dirt-producing" gangue minerals. Under the present arid climate at Iron Mountain, disintegration would be expected to prevail over decomposition.

Since the ore samples tested for susceptibility were

taken from the surface layers of the orebodies, significant error may have been introduced by considering the mean susceptibility of the samples as representative of the entire orebodies. According as the mean susceptibility used was too low or too high, orebodies F, F_1, and G would be, respectively, more or less oblate than calculated.

Analysis of the Anomalies over the Alluvium

Positive anomaly Δ, with peak magnetic values atop the hill containing orebody A, appears to be unipolar, because the negative outer extremes surrounding it are indistinct. This indicates a considerable depth to its negative pole. The spread and elongation of the isogams to the southeast together with their large magnitude suggest that orebody A is an elongate, thick mass that dips southeastward beneath limestone and alluvial cover. (See cross section x-x'.) On the eastern slope of the hill, no magnetite-rich talus covers the limestone, and ferruginous veins transect the limestone only locally. Except for a thin veneer of magnetite-rich talus that has slid down from orebody A*, the alluvium contains but little iron ore float. Thus, the contribution of the exposed surface rocks to anomaly Δ is negligible. Anomaly Δ must result entirely from the hidden extension of orebody A. The wide spread of the isogams over

the central part of the anomaly, and the crowding of them near the periphery point to a flat or tabular disturbing body. The large anomalies associated with anomaly Δ persist toward orebody A°. This may mean that orebody A merges with orebody A° beneath limestone cover.

According to Koenigsberger (10), "The outer negative (northern) extreme is as large or larger than the central extreme, if a magnetic oblate spheroid dips 10°- 20° to the magnetic south, and if it dips between such angles to the north the (outer) negative extreme lies south and is weaker than the central extreme ..... The dipping of an oblate ellipsoid or elliptic cylinder makes the isanomalies come nearer together on the higher side than on the lower dipping side." Since this information refers to the induction produced by a magnetic field having an inclination similar to that at Iron Mountain, and if it can be extended to include an elongate body, it can aid in the interpretation of anomalies Σ and ϕ. The fact that negative anomaly ϕ is about the same magnitude as positive anomaly Σ indicates that the disturbing mass is flat and that it dips at a shallow angle. The fact that the negative extreme of anomaly ϕ lies to the magnetic north of the positive extreme of anomaly Σ signifies that this mass dips to the magnetic south. (See cross section z-z'.) The crowded isogams between the two anomalies probably represent the high side of the disturbing mass. The elongation of the isogams to the southeast suggests a blade-like shape for the disturbing mass. Although the spreading apart of the isogams to the

southeast probably indicates a greater depth to the disturbing mass, some of the spreading could be due to a decrease in the thickness of the mass.

Anomaly Λ consists of an eastern lobe and a southeastern lobe. Both lobes probably signify the extension of orebody C beneath alluvial cover. The eastern lobe merges with anomaly Σ, and may well indicate a continuous layer of ore extending from orebody C to anomaly Σ. The extreme crowding of the isogams toward the periphery of the southeastern lobe indicates a very shallow depth to the disturbing mass. It is certain that part of, if not all, the magnitude of the southeastern lobe results from surface material, for a bench of iron-rich talus standing several feet above the surrounding alluvium coincides with the magnetic contours of the southeastern lobe. Anomaly θ is probably a composite of the negative poles associated with anomalies Λ and Σ.

The circularism of the isogams of anomaly ω would indicate considerable depth to the disturbing body were it not for the fact that the small exposure of ore (shown by dashed lines on the anomaly map) to the northwest probably represents the surface expression of the disturbing body. The crowding of the isogams to the west and their spread to the east probably indicate an easterly dip. The small positive anomaly northeast from hill β may be due to a small orebody. (See cross section Z-Z'.) Negative

anomaly P2 is probably a composite south pole associated with anomaly ω and the northwestern extension of anomaly Σ.

The crowding of the isogams of anomaly P3 to the west-southwest and their spread to the east-northeast suggest that the disturbing body dips to the east-northeast. The rather large negative pole to the magnetic south indicates that this body is flat and shallow and that it has a low dip.

The spacing of the isogams of anomaly Ψ suggests a body elongate to the southeast and dipping to the southeast or east.

The depths to the centers of the disturbing bodies were calculated from platform data and from depth rules described by Nettleton (9). Since these methods tend to yield the maximum possible depths to the disturbing bodies, the true depths are generally less than the calculated depths. Since the anomalies due to separate disturbing masses overlap one another, and since the horizontal polarization has been ignored, the calculated depths are only rough approximations of the maximum depths.

Over positive anomaly Σ at P1, the anomaly recorded atop the platform, which was 11.7 feet high, was 380 gammas less than the anomaly of 2220 gammas recorded at its base. The disturbing body was compared to a sphere and then to an infinite horizontal cylinder, for its actual shape is a composite of these two figures. If it is assumed that

the anomaly decreases inversely as the cube of the distance from the center of the disturbance, the case for a vertically magnetized sphere, a depth of 180 feet is obtained. If it is assumed that the anomaly decreases inversely as the square of the distance from the center of the disturbance, the case for an infinite horizontal cylinder, a depth of 120 feet is obtained. Transverse to the elongate axis of the disturbance, the distance between the peak anomaly and the half-value of the peak anomaly is about 85 feet. Since the ratio of this distance to the depth is $\frac{1}{2}$ for a sphere, a depth of 170 feet is obtained for a spherical approximation; and since this ratio is 1/2.05 for an infinite horizontal cylinder, a depth of 165 feet is obtained for a cylindrical approximation. The true depth is probably less than the mean of these maximum depths.

Over the positive anomaly at P3, the anomaly recorded atop the platform was 1800 gammas less than the anomaly of 4100 gammas recorded at its base. The inverse-cube law of variation gives a depth of 60 feet. Hence, the disturbing mass is shallow and has a maximum possible depth of about 60 feet. The isogams indicate that the disturbance analyzed is only the upper protuberance of a larger disturbance.

If the matter producing the anomalies over the alluvium lies within the basement beneath the alluvium, this basement must be quite shallow, and variable in composition.

It is more probable that the alluvial anomalies are caused by either concentrations of magnetite-rich talus within the alluvium or by discrete orebodies. If the hypothesis of magnetite-rich talus holds true, the disturbing bodies are probably contiguous with the surface, and may hence be analyzed by the graphs for surface-contacting ellipsoids. The use of the graphs to estimate the volume concentration of magnetite on the assumption that it is directly proportional to the susceptibility is valid only for low susceptibilities. If the anomalies over the alluvium are considered to result from localized concentrations of magnetite-rich talus, the mean susceptibility of such concentrations would be low and the use of the graphs to determine the concentrations would be valid.

In order to estimate the concentration of magnetite-rich talus which could produce anomaly Σ, the disturbing body was assumed to be a prolate ellipsoid with a horizontal axis of revolution. The axial ratio, determined by noting the position of the isogam equal to 1/10 the central positive extreme (see Koenigsberger (10)) is about 3. For an axial ratio of 3 and a mean central anomaly of 2000 gammas, figure 9 yields a susceptibility of 0.0067. On the assumption that the effective susceptibility of disseminated magnetite is 0.203 [†], a magnetite

[†] For the calculation of this figure for the effective susceptibility of disseminated magnetite, see note 4 in the appendix.

concentration of 3.3 percent is obtained.

Most theoretical treatments of magnetic anomalies involve the maximum possible depth to the center of the disturbing matter, and, accordingly often give results indicating the maximum possible volume and the minimum possible susceptibility contrast. If the depth to the center of a disturbing body is accurately located, but its peak is not contiguous with the ground surface as assumed, the estimate of the magnetite concentration will be too small and the estimate of the volume of the disturbing body too large. The same holds true if the depth to the center of a surface-contacting body is assumed too deep. The magnetite concentration of 3.3 percent calculated as producing anomaly Σ is, therefore, a minimum estimate. Since the ore breccia consists of more hematite than magnetite, its concentration beneath anomaly Σ must be much greater than 3.3 percent. The ratio of hematite to magnetite can be roughly estimated from the fact that the mean susceptibility of the ore specimens tested (see fig. 7) is less than the susceptibility of polished specimen C255, which contained 25 percent magnetite, and more than the susceptibility of polished specimen C253, which contained 15 percent magnetite. Application of linear interpolation to these data yields a hematite-magnetite ratio of about $4\frac{1}{2}$. If this ratio is correct, the minimum concentration of ore breccia beneath anomaly Σ must be at least 15 percent. A concentration of 15 percent

seems much too high to be ascribable to talus derived from the exposed orebodies. From surface evidence it seems doubtful that the concentration of iron ore in the alluvium could exceed 5 percent. If, on the other hand, anomaly Σ and the other large positive anomalies over the alluvium are assumed to be caused by solid orebodies, their large magnitude and the fact that they bear no relation to the present drainage pattern, but reflect the southeastward continuation of the surface orebodies are more reasonably explained.

That the large ratio of hematite to magnetite characterizes the entire orebodies and not just their surfaces is corroborated by the result of the resistivity measured for orebody D after a slight rainfall. From the data obtained from a "Wenner" electrode arrangement set for 50 feet of depth penetration, a resistivity of 3×10^4 ohm-cm was calculated. This value lies considerably outside the range from 1 to 100 ohm-cm commonly observed for ores containing a predominance of magnetite.

Estimate of the Ore Reserves beneath Alluvial Cover

On the basis of drill-hole data obtained from orebodies C, D, and E, the U. S. Geological Survey (1) has calculated that the orebodies exposed on the hills of Iron Mountain

contain 5,175,000 tons of indicated† ore and about 300,000 tons of inferred† ore. The results of the magnetic survey substantiate the configuration of the surface orebodies portrayed by the U. S. Geological Survey. However, two very small surface orebodies, not shown on Gilluly's map, were discovered by the use of the magnetometer and confirmed by noting iron ore in situ. On the anomaly map, the boundaries of these two orebodies are shown by dashed instead of dotted lines. One is southeast from orebody E and the other is southeast from orebody G. The results of the magnetic survey indicate the presence of a much greater amount of ore beneath alluvial cover than could be estimated from the drill-hole data. Accordingly, the estimate of ore reserves at Iron Mountain can be considerably increased.

Minimum, maximum, and "reasonable" estimates of inferred ore were made for anomalies Σ, ω, P3, and ψ; whereas, only "reasonable" estimates were made for anomalies Δ and Λ. (See table 3.)

The specific gravity of the ore was assumed to be 4.4 in the tonnage calculations. This value represents the mean specific gravity of 25 ore samples tested in the laboratory.

The anomalies were smoothed out in order to eliminate higher order features. The effects of the localized peak values of anomalies P3 and ψ were practically eliminated in

†The terms "indicated" and "inferred" accord with the usage prescribed for them by the U. S. Bureau of Mines.

the process. Anomaly Σ was separated from anomaly Λ.

Table 3. Estimates of inferred ore beneath alluvial cover in long tons:

Anomaly	Minimum estimate	Maximum estimate	Reasonable estimate
Σ	620,000	1,400,000	920,000
ω	610,000	1,700,000	1,040,000
P3	150,000	320,000	220,000
ψ	80,000	580,000	220,000
Δ (extension of orebody A)	-	-	4,900,000
Δ (extension of orebody A°)	-	-	1,100,000
Λ	-	-	1,600,000
		Total	10,000,000

The minimum estimates were made by assuming that the disturbances were surface-contacting, oblate ellipsoids with vertical axes of revolution. For each disturbance, the mean radius of the isogam equal to 1/10 of the central peak anomaly was used as the length of the transverse axis, a procedure which is justifiable as long as the isogams are not too elongated. The axial ratio which would give the observed peak anomaly for a susceptibility of 0.135[†] was then found in figure 8, and the length of the axis of revolution computed. The axial ratios obtained ranged from

[†]This is the mid-value of the interval from 0.10 to 0.17, an interval in which the mean susceptibility of 14 solid ore samples tested in the laboratory most probably lies.

about 1/10 to 1/20, thus indicating very flat disturbances. Because of such flatness, the positive isogams would virtually outline the true size of each disturbing body. The lengths of the principal axes of revolution having been determined, the volumes of the ellipsoids were computed. Multiplying these volumes by the density gave the minimum tonnage estimates.

In order to calculate the maximum possible volume of the disturbing masses, it is necessary to find the configuration of disturbing matter at depth which will produce the peak central anomalies observed at the surface. If the material at depth is similar in shape and composition to that exposed at the surface, it should be possible to place constraints upon the allowable configuration of material at depth which can produce a given anomaly. For this purpose, the ratios of the anomalies expected at depth to those expected for surface contact were computed from equations derived from more elaborate equations given by Koenigsberger (10). The values obtained were plotted as a function of the depth and of the ratio of the principal axes. Figure 11 gives the ratio of the peak anomaly at depth to that for surface contact for oblate ellipsoids with vertical axes of revolution, and figure 12 gives this ratio for prolate ellipsoids with horizontal axes of revolution. Equation 5.3 was used to obtain figure 11, and equation 5.4 was used to obtain figure 12.

$$5.3 \qquad \frac{\Delta Z_h}{\Delta Z_o} = \frac{\operatorname{arctg}\left(\frac{\sqrt{b^2 - a^2}}{h}\right) - \frac{h\sqrt{b^2 - a^2}}{h^2 + b^2 - a^2}}{\operatorname{arctg}\left(\frac{\sqrt{b^2 - a^2}}{a}\right) - \frac{a\sqrt{b^2 - a^2}}{b^2}}$$

$$5.4 \qquad \frac{\Delta Z_h}{\Delta Z_o} = \frac{\ln\left|\frac{\sqrt{h^2 + a^2 - b^2}}{h} + \sqrt{a^2 - b^2}\right| - \frac{(h^2 - a^2 + b^2)\sqrt{a^2 - b^2}}{h\sqrt{h^2 + a^2}}}{\ln\left|\frac{a + \sqrt{a^2 - b^2}}{b}\right| - \frac{(2b^2 - a^2)\sqrt{a^2 - b^2}}{ab^2}}$$

where a = length of the axis of revolution
b = length of the transverse axis
h = depth to the center of the ellipsoid

In both figures 11 and 12, the ordinate represents the anomaly ratio, the abscissa represents the ratio of the depth to the vertical axis of the ellipsoid, and the ratio of the principal axes serves as a parameter for a family of curves.

In both figures, the power of the anomaly variation with depth is asymptotic to the inverse cube. This corresponds to the approach of the isogams to circles as the depth to a disturbance increases. In figure 11, for a constant anomaly ratio, the power of the anomaly variation with depth changes from the inverse cube to zero as the axial ratio decreases from 1 to 0. In figure 12, for a constant anomaly ratio, the power of the anomaly variation with depth changes from the inverse cube to the inverse square as the axial ratio increases from 1 to ∞.

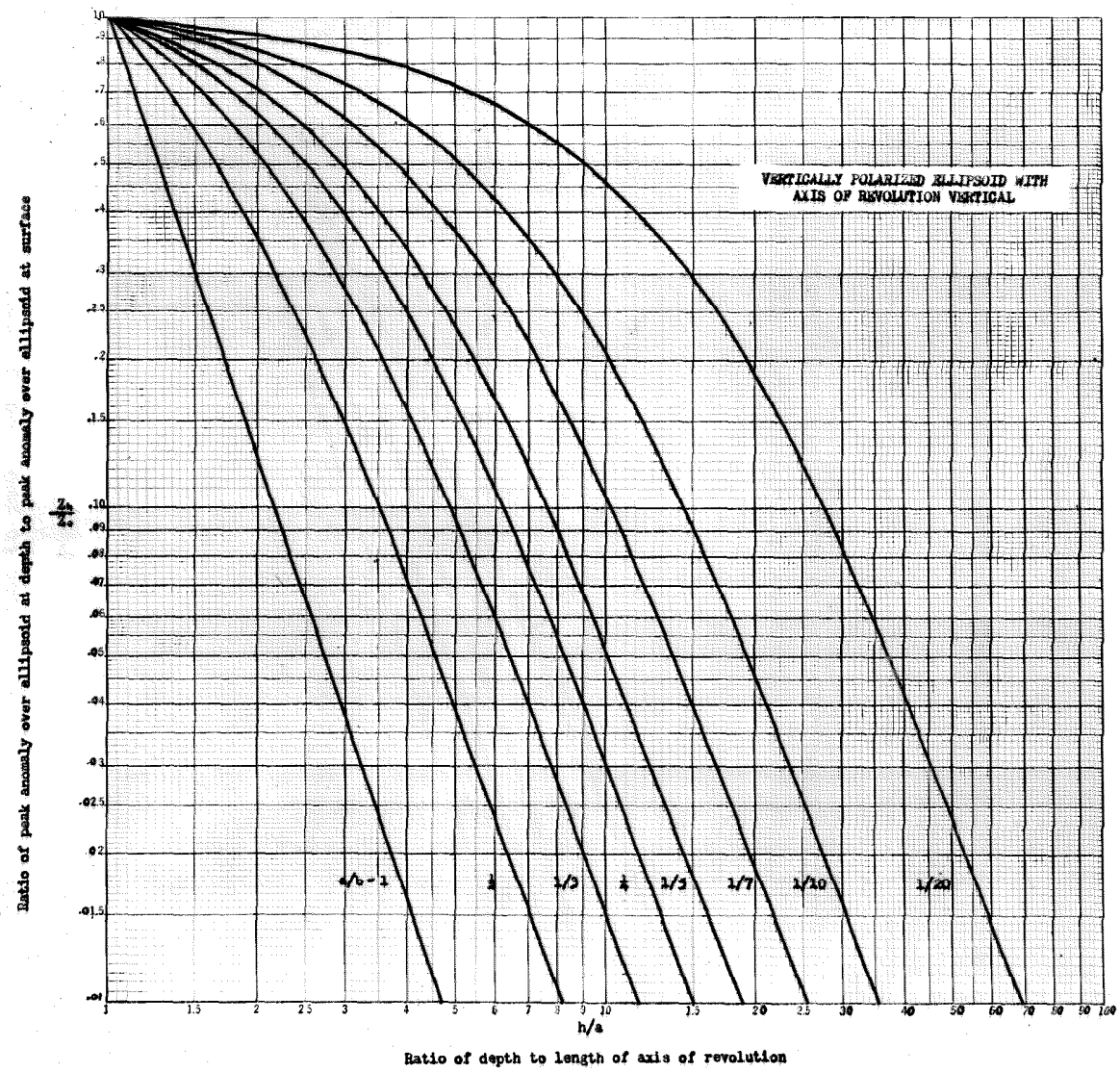
VERTICALLY POLARIZED ELLIPSOID WITH
AXIS OF REVOLUTION VERTICAL
Ratio of peak anomaly over ellipsoid at depth to peak anomaly over ellipsoid at surface
h/a
Ratio of depth to length of axis of revolution
a/b = 1
1/3
1/5
1/7
1/10
1/20

Figure 11.

Figure 12.

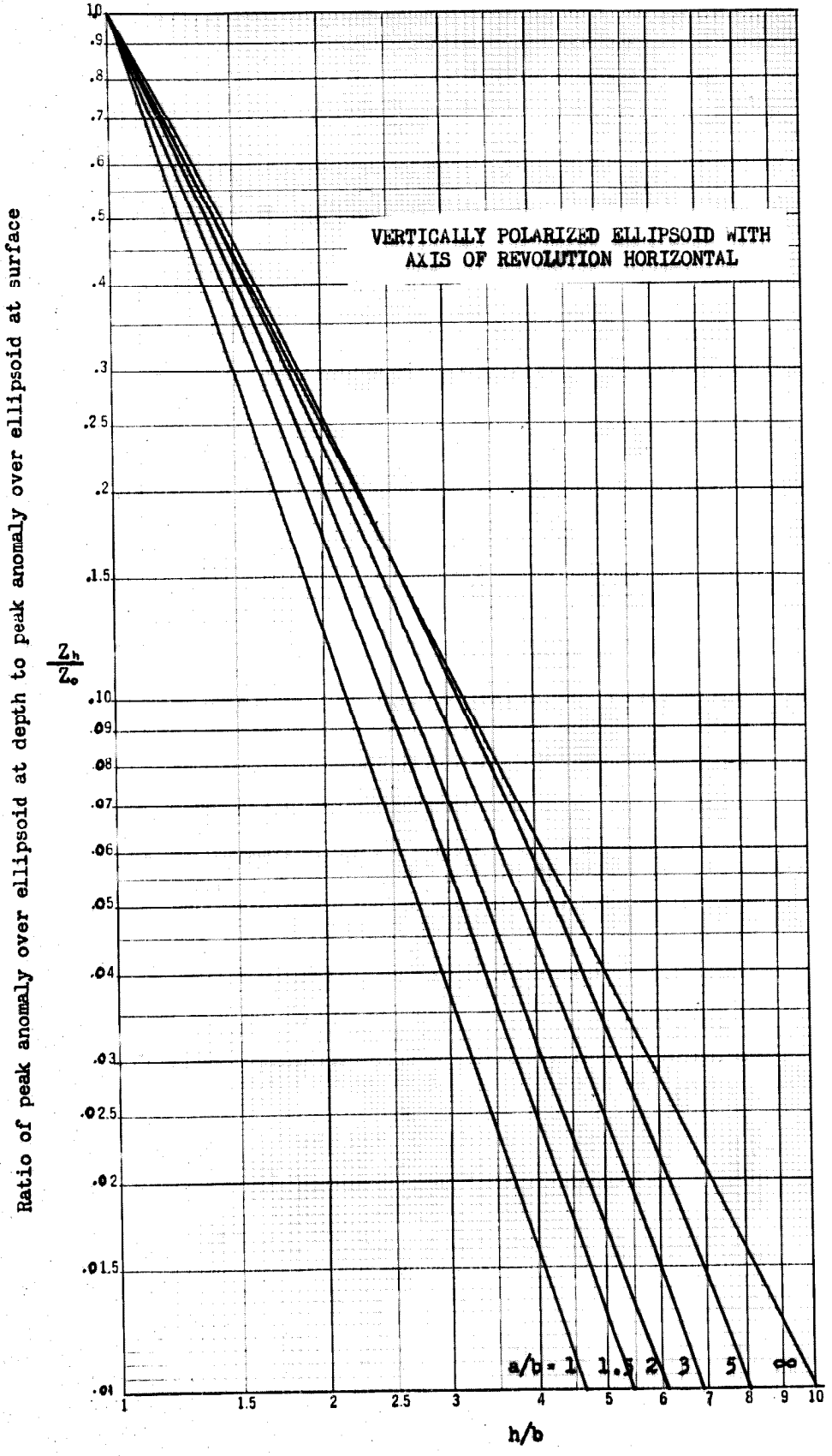
VERTICALLY POLARIZED ELLIPSOID WITH
AXIS OF REVOLUTION HORIZONTAL
Ratio of peak anomaly over ellipsoid at depth to peak anomaly over ellipsoid at surface
$\frac{Z_h}{Z_o}$
1.0
.9
.8
.7
.6
.5
.4
.3
.25
.2
.15
.10
.09
.08
.07
.06
.05
.04
.03
.025
.02
.015
.01
a/b = 1 1.5 2 3 5 ∞
1 1.5 2 2.5 3 4 5 6 7 8 9 10
h/b
Ratio of depth to length of transverse axis

Although the curves in figure 12 for $a/b>5$ cross over the curves for $a/b=\infty$, the slopes of the former do not appear steep enough to indicate a power variation with depth exceeding the inverse cube.

The maximum estimates for anomalies Σ, ω, P3, and ψ were determined by finding the prolate ellipsoids at depth which could produce the observed anomalies. The depths were determined by application of half-peak value rules to the smallest diameters of the isogams. Platform data were not used to obtain the depths because, for shallow bodies, the platform method gives the depth to the highest prominence of an orebody, whereas, the half-peak value rules give a depth more representative of the entirety of an orebody.

The anomaly ratio was determined for anomaly Σ by comparing its central peak anomaly with that found over orebody D, which is probably similar in shape to the body producing anomaly Σ. This ratio was determined for anomalies ω, P3, and ψ by comparing their peak anomalies with the mean of the peak anomalies found over orebodies F and G. For each anomaly, the axial ratio was calculated as the ratio of the maximum to the minimum radius of the isogam equal to 1/10 of the central positive anomaly. In figure 12, the ratio of the depth to the transverse radius was read off the abscissa. Then, the lengths of the principal axes, the volume, and the mass of the disturbance were computed.

For the determination of the maximum volumes, figure 12,

for prolate ellipsoids, was preferred to figure 11, for oblate ellipsoids, because:

1. For a given width of the isogam equal to half the peak value, the half-peak value rules give depths to a sphere and to an infinite horizontal cylinder differing by only $2\frac{1}{2}$ percent. Since with varying eccentricity, prolate ellipsoids of revolution are bounded by a sphere and an infinite horizontal cylinder, the assumption of either a sphere or an infinite horizontal cylinder causes but little error in the determination of the depth to a prolate ellipsoid. On the other hand, the half-peak value rules for the determination of depth to shallow oblate ellipsoids are difficult to compute and are quite sensitive to the ratio of the principal axes. Since some flattening is probable, the depths used are too large, and, accordingly, too much ore will be indicated.

2. For any given anomaly ratio and depth, there correspond three ellipsoids of different shape having the same volume. At shallow depths two "isovolumes" occur as roots on figure 11, and one on figure 12. At large depths, two "isovolumes" occur as roots on figure 12, and one on figure 11. The region of the two graphs used for the analysis of anomalies Σ, ω, P3, and ψ was such as to give a larger volume for the assumption of a prolate ellipsoid than for an oblate ellipsoid.

3. The fact that orebodies D, G, and F are flattened tends to render the assumed anomaly ratios too large; this, in turn, has the effect of further making the volume indicated too large. However, comparison of figure 8 with figure 9 shows that for mild flattening, the effect is negligible.

Figure 11 did not aid directly in the maximum ore estimates, but is presented for the sake of completeness. If the depth to the center of the alluvial disturbances were ever accurately determined, figure 11 would then be more useful.

In table 3, the ratios of the maximum to minimum estimates are of large magnitude. In order to reduce the magnitude of possible error, the geometrical mean of the minimum and maximum estimates was used to give the "reasonable" estimates.

In order to give the volume used for the calculation of the "reasonable" estimate of ore beneath anomaly Λ, the area included by the 1000 gamma contour was multiplied by the thickness of the ore beds indicated directly by the drill-hole data. The same was done for anomaly Δ, except that the thickness of the ore bed was inferred from cross section x-x'.

Structure and Geologic History

Because of their rather massive appearance, inspection of the breccias themselves gives little indication as to whether they are of sedimentary or tectonic origin. Within

the gray limestone breccias are brown ferruginous inclusions which consist of patterns of fragments distinctly separated from one another by the limestone. The "exploded" appearance of these inclusions may point to a tectonic origin for the breccias. However, it is also possible that the "exploded" appearance may represent metasomatic replacement by limestone along fissures which formed within larger inclusions.

Strong evidence for a sedimentary contact between the upper breccia layer and the conglomeratic sandstone was noted in hill α. Several feet below the contact, the sandstone contains rounded to sub-angular limestone cobbles and pebbles, the quantity of limestone increasing and the size of the particles decreasing upward to the contact. The cobbles and pebbles are clearly separated from each other and do not appear to represent nodules weathered from massive limestone. Although the contact is very irregular on a small scale, its general appearance is planar and it has a shallow dip. The divergence between the contact and the dip of the strata beneath is about 5°. Above the contact, the limestone changes upward from cobbly material into massive breccia. The matrix between the limestone cobbles above the contact consists primarily of siltstone; whereas, the limestone cobbles below the contact are interspersed with siltstone, sandstone, and an assemblage of igneous and metamorphic cobbles of a wide range of composition.

Farther below the contact, there is sandstone which is yellow to gray, arkosic, and which ranges from thin silts to coarse conglomerates with boulders six feet in diameter. The massive limestone breccia above the contact is not homogeneous, but consists of angular fragments of all sizes demarked by various shades of gray.

Because the contact between the ore-bearing breccias and the lower sandstone layer is nowhere exposed, the nature of the contact is unknown.

The selection of two layers of sedimentary breccia rather than the single layer of tectonic breccia shown on the geologic maps of Lamey and Gilluly (1) is based upon the following evidence:

1. The contact in hill α appears to be gradational.

2. The upper layer of breccia consists almost wholly of limestone. Veins of ferruginous minerals transect it only locally. The postulate of a single layer of breccia requires an exceedingly abrupt southeastward termination of the iron ore and other breccias.

3. Cross sections of Iron Mountain drawn on the basis of two layers of breccia agree more reasonably with the dips and strikes recorded at the surface and eliminate the necessity for postulating complex faulting.

4. About a mile to the east of Iron Mountain are two limestone ridges that dip eastward at a shallow angle and extend parallel for more than a mile. Considering

these ridges to be cuestas is far more tenable than considering them to be a single layer of fault outliers.

5. The magnetic anomalies over the alluvium indicate that some of the orebodies extend southeastward beneath alluvial cover and must lie beneath and not be underlain by a certain layer of sandstone. The magnetic anomalies further indicate that the orebodies isolated beneath the alluvium must have a southeastward elongation and dip, and must be rather flat. This reflects a continuation of the structure of the orebodies exposed on the hills.

The bedding attitudes recorded at the surface indicate that the prevailing dip is southeastward and that the dip and the intensity of folding increase toward the crystalline-complex. Analysis of the isogams indicates that a southeastward dip together with mild folding continue beneath alluvial cover. Although the general spreading apart of the isogams to the southeast probably indicates an increase of depth to the center of the disturbing matter, it must be held in mind that for any configuration of an orebody at depth, there is a surface distribution of matter which can produce an identical anomaly.

The four faults shown on the anomaly map have the feature in common of striking southeast.

Fault m-m' consists of a zone of green, slickensided, and brecciated material several feet thick, separating

igneous rocks to the southwest from sediments to the northeast. The fault appears to dip at a steep angle to the northeast. The appearance of the outcrops between fault m-m' and orebody A suggests a series of parallel fault slices. Some of the igneous rocks in these "slices" are quite massive, and appear to be more related to the crystalline-complex than to the breccias. The igneous rocks southwest of fault m-m' are a loose assemblage of talus forming a horizontal outcrop line about the surrounding hills. They may represent Quaternary terrace gravels eroded from the crystalline-complex.

Fault q-q' separates andesite to the southwest from quartz monzonite to the northeast. Its trace is marked by a zone of green, brecciated material. The straightness of its trace suggests a steep dip.

Fault p-p' is well exposed along its northwestern extent, where it separates the crystalline-complex from the tertiary sediments and breccias. It dips about 45° to the northeast, and a zone of green brecciated material can be traced along much of its length. It appears to have displaced orebody A* several hundred feet southeast from orebody A.

Geologic, drill-hole, and magnetic data confirm the presence of fault r-r' or at least a sharp northeastern boundary to orebody D. (See fig. 10.) The consistently large negative anomalies along fault r-r' are equal to

nearly half the magnitude of the positive anomalies along the crest of orebody D. This indicates that orebody D terminates abruptly northeast from fault r-r'. The fact that the large negative anomalies surrounding orebody D are situated well above the lowest outcrop line of the ore indicates proximity to the negative pole of the orebody and thus confirms its shallow depth.

The over-all appearance of the exposed orebodies is that of tabular masses elongate and dipping to the southeast. Anomaly Σ probably signifies the southeastward extension of orebodies F' and F beneath alluvial cover. Anomaly ω appears similarly related to orebody G. Anomalies P3 and Ψ do not appear to represent the continuation of any particular surface orebody. The fact that several of the exposed orebodies cap hills which are proximal to one another suggests that they are erosion remnants of larger, continuous masses. Such may be the association of orebodies F', F, and G, and also the association of orebodies H and K.

The large negative anomaly in the ravine between orebodies C and D indicates a complete separation of these orebodies from each other. The contours of this negative anomaly appear crowded toward orebody C; this indicates that the south pole of orebody C is closer to the alluvial surface than the south pole of orebody D. This is to be expected, for as a result of the horizontal component of magnetization, the negative extreme appears to the north

of a magnetic body and a much weaker negative anomaly appears to the south of it.

Figure 13 is a reproduction of an east-west cross section through orebodies B and C made by the U. S. Geological Survey (1).

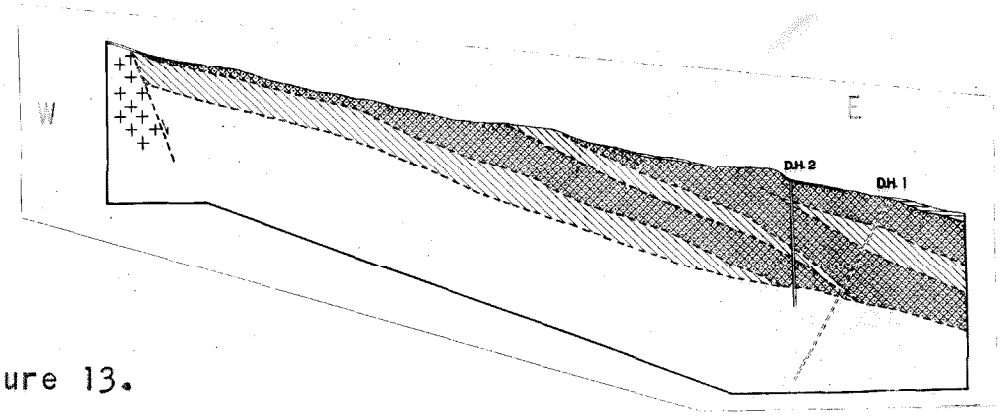

Figure 13.

Although they are apparently separated at the surface, the two orebodies are shown as belonging to a group consisting of several layers of ore. The downslope part of the group was constructed upon the basis of data obtained from two drill holes. The fact that the anomaly over orebody B has a much smaller magnitude than that over orebody C corroborates the upward thinning of the ores inferred by the U. S. Geological Survey.

The eastward bend of the magnetic contours located west from orebodies B, C, and D may be partially drainage controlled, but probably reflects the arc of negative anomalies expected to conform to these orebodies.

The following brief account of the history of Iron

Mountain suggests itself on the basis of the results obtained. This outline is sketchy because a much wider geological study would have to be made before a more complete history of the Mountain could be outlined.

1. Limestone strata were replaced locally by magnetite as a result of contact metamorphism produced, presumably, by intrusion of quartz monzonite.

2. The metamorphosed limestone together with rocks of entirely different composition were elevated. Alternate layers of breccias and arkosic conglomeratic sandstone were deposited during the Tertiary under arid conditions. The breccias were laid down as an irregular series of overlapping lenses of rockslides or debris flows, or both.

3. The breccias were cemented by the solution and redeposition of their calcareous and ferruginous constituents.

4. The uplift of the crystalline-complex produced upbowing and folding of the entire sedimentary series. This was accompanied by steep-angle faulting trending southeastward. The faulting brought slices of the crystalline-complex adjacent to the sediments, and offset a large orebody. The faulting generally followed the plane of weakness afforded by the presence of soft conglomeratic sandstone between the competent crystalline-complex and the breccias.

5. Regional uplift occurred. Terrace gravels were

left stranded. The tongues of limestone, iron ore, and other breccias were eroded through; this left as remnants isolated knolls and ridges capped by resistant breccias. The source rocks of the breccias have been either completely eroded away or else lie outside the region investigated.

6. Possibly, lightning struck the high points of the orebodies, thus producing surficial remanent magnetism. Perhaps, the present day formation of talus tends to disorient the polarization of the magnetized layers, and thus causes the effects of induction by the present magnetic field of the earth to predominate over those of remanent magnetization.

APPENDIX

Note 1.

For the small magnet, there was no perceptible difference between the S/N and N/S positions. However, for the medium and the large magnets, the N/S positions show values slightly larger than the S/N positions, a fact which probably results from the dipole moments of these two magnets not being exactly symmetrical about their threaded centers. Effects of induction on the auxiliary magnets by the vertical component of the earth's field would be expected to have an effect opposite to that observed for the medium and large magnets.

If the field intensity of the auxiliary magnets were to vary inversely as a constant power of the distance from their centers, the curves in figure 3, drawn on semi-log coordinates, would be straight lines. The curves are concave upward, the 34 centimeter position corresponding to an inverse power variation with distance of about 2.95, and the 25 centimeter position corresponding to an inverse power variation with distance of about 2.80. This is explained by the fact that the magnets tend to obey the inverse-cube law of variation with distance when far from the knife edges; and the inverse-square law of variation with distance when one pole is much closer to the knife edges than the other. Further complications arise from the fact that since the

poles of the paired needles do not lie on the vertical axis of the instrument, only a component of the field of the auxiliary magnets will react with them, an effect which increases with the approach of the auxiliary magnets toward the knife edges.

The empirical determination of the gamma values for the various positions of the magnets is superior to those methods which involve the finding of the moments of the magnets and the calculation of the fields expected at various distances therefrom, because the latter method is based on the assumption that the magnets perform as remote dipoles, an assumption which, as shown by the curves of figure 3, tends to introduce considerable error.

Note 2.

The coil constant of a double-solenoid, which is the ratio of the axial field intensity to the current through the windings, is

A.1 $$\frac{H}{I} = \frac{4\pi n}{10}\left[1 - \left(\frac{d_1^2 + d_2^2}{32}\right)\left(\frac{1}{x^2} + \frac{1}{(L-x)^2}\right)\right]$$

L, x, and $(L - x) >> d_1$ and d_2

where		For the large double-solenoid	For each half of the Einstein-de Haas coil
n =	turns/cm for all layers	= 40.9 turns/cm	= 57.10 turns/cm
d_1 =	diameter of outer layers	= 15.0 cm	= 6.57 cm
d_2 =	diameter of inner layers	= 8.5 cm	= 5.20 cm
L =	length of the solenoid	= 90.5 cm	= 25.0 cm
x =	axial distance from one end of the solenoid		

Numerical substitution into equation A.1 gives a coil constant of 50.98 gauss/ampere at the center of the large double-solenoid, and 50.85 gauss/ampere at points 12.5 cm from this center, points which coincide with the centers of each of the two parts of the Einstein-de Haas coil. Since this represents a variation of only 0.24 percent of the coil constant, the field produced by the large double-solenoid is essentially uniform throughout the length of the Einstein-de Haas coil.

Application of equation A.1 to the Einstein-de Haas coil yields a coil constant of 70.57 gauss/ampere at the center of each of its symmetrical halves. The drop in value at a distance 3.5 cm from the centers, a distance corresponding to the amount which the sample tubes projected in their rest position on both sides of the centers, is 0.8 percent. The effective coil constant throughout the length of the samples was taken as the arithmetic mean of the center and 3.5 cm off-center values, namely, 70.30 gauss/ ampere.

The reduction in coil constant at the center of one part of the Einstein-de Haas coil by the reaction of the adjacent, opposing part amounted to 1.2 percent. After it was corrected for this reaction, the effective coil constant became 69.45 gauss/ampere, a value which was used in subsequent calculations.

The pitch of the windings for both the large double-solenoid, and the Einstein-de Haas coil was so small that radial components of field intensity within them could be entirely neglected.

Note 3.

The use of the test coil as an intermediary device with which to calibrate the galvanometer depends upon the fact that when a current is passed through it, it behaves as a dipole. When it is pulled through the Einstein-de Haas coil it produces a definite flux, determined by the effective dipole moment of the test coil and the coil constant of the Einstein-de Haas coil.

In order to calibrate the test coil, galvanometer sensitivity was reduced until the flux generated by the Hibbard Standard was within range of the galvanometer scale. The test coil, through which a known current was passed, was then pulled from the center of one part of the Einstein-de Haas coil to the center of the other part as was done with the powdered specimens, the resultant galvanometer deflection noted, and the effective turns times area, NA, of the coil computed. The formula for NA is derived as follows:

$$\text{A.2} \qquad \frac{2\Upsilon M_{tc}}{D_{tc}} = \frac{\Phi_{hs}}{D_{hs}}$$

where M_{tc} = magnetic moment of the test coil
2Υ = coil constant of the Einstein-de Haas coil allowing for double deflection = 2 x 69.45 gauss/ampere
D_{tc} = galvanometer deflection due to the test coil
D_{hs} = galvanometer deflection due to Hibbard Standard
Φ_{hs} = flux of Hibbard Standard = 75,170 lines

Substituting INA for M_{tc} into equation A.2, where I equals the current, N the turns, and A the cross sectional area of the coil, and solving for NA gives

$$A.3 \qquad NA = \frac{D_{tc}\,\phi_{hs}}{I D_{hs}\,2\pi}$$

Substitution of experimental values and constants into equation A.3 gives NA = 720 turns-cm^2.

The galvanometer was then adjusted to its more sensitive setting used for the measurement of the magnetic moment of the powdered specimens. A current low enough to be within the range of full scale galvanometer deflection was then passed through the test coil and the deflection produced produced by moving it through the Einstein-de Haas coil again noted. The galvanometer sensitivity, c, was then calculated from

$$A.4 \qquad c = \frac{INA}{D_{tc}}$$

using the effective value for NA calculated from equation A.3.

The effective value for NA of 720 turns-cm^2 is only 0.7 percent more than the value of 715 turns-cm^2 calculated from the geometry of the test coil. However, the effective value of NA would be expected to be a little lower than the theoretical value, for a finite time is required to pull the test coil through the Einstein-de Haas coil, a delay which tends to reduce the peak swing of the galvanometer. The effective rather than the theoretical value of NA was used

for the calibration of the galvanometer scale because the terminal effect of the input wires to a coil is often equivalent to a sizable fraction of a turn. Since the test coil had only 61 turns, the unknown terminal effect might introduce appreciable error in a theoretical determination of NA.

The test coil had an axial length comparable to that of the powdered specimens and was pulled through the Einstein-de Haas coil at approximately the same rate as were the powdered specimens. This helped to compensate for the error resulting from the fact that a finite time is required to move the specimens through the coil.

Note 4.

The figure used for the effective susceptibility of disseminated magnetite was obtained from the following formula:

A.5 $$k' = \frac{k_o}{1 + k_o\lambda} = 0.203$$

where k_o = true susceptibility = 1.35 for pure magnetite in a field of 1 oersted, the magnetite having been prepared by roasting. (See the International Critical Tables (11).)
λ = demagnetizing factor = $4/3\ \pi$ for a sphere

Since the effective susceptibility of disseminated magnetite is only slightly dependent on the susceptibility of solid magnetite, the value used for k_o in equation A.5

did not need to be precise. This arises from the fact that as the true susceptibility approaches infinity, the effective susceptibility is asymptotic to the reciprocal of the demagnetizing factor. The asymptotic value is 0.239 for spherical particles. The assumption that the mean shape of disseminated magnetite particles may be approximated by a sphere is based upon the fact that magnetite crystallizes in the isometric system and the fact that it has no pronounced cleavage planes.

REFERENCES

1. CARL A. LAMEY (and JAMES GILLULY), Iron Mountain and Iron King Iron-ore Deposits, Silver Lake District, San Bernardino County, California. California Division of Mines Bulletin 129 (1948), p. 41.

2. C. A. HEILAND, Geophysical Exploration (1946), pp. 303-328.

3. W. R. SMYTHE, Static and Dynamic Electricity (1939), p. 267.

4. A. C. JOHNSON and SPANGLER RICKER, Summary of Investigations of the Iron-ore Deposits of California. California Division of Mines Bulletin 129 (1948), p. 237.

5. W. H. NEWHOUSE and J. P. GLASS, Some Physical Properties of Certain Iron Oxides. Economic Geology Vol. XXI (1936), p. 699.

6. R. M. BOZARTH and D. M. CHAPIN, Demagnetizing Factor of Rods. Journal of Applied Physics Vol. XIII (1942), p. 320.

7. A. G. WEBSTER, The Theory of Electricity and Magnetism (1897), p. 374.

8. L. L. NETTLETON and T. A. ELKINS, Relations of Magnetic and Density Contrasts to Igneous-rock Classifications. National Research Council (American Geophysical Union) Part IV (1944), p. 662.

9. L. L. NETTLETON, Geophysical Prospecting for Oil (1940), p. 224.

10. J. KOENIGSBERGER, Zur Deutung der Karten Magnetischer Isanomalen und Profile. Beitrage zur Geophysik (1928), p. 242.

11. International Critical Tables Vol. VI (1929), p. 375.

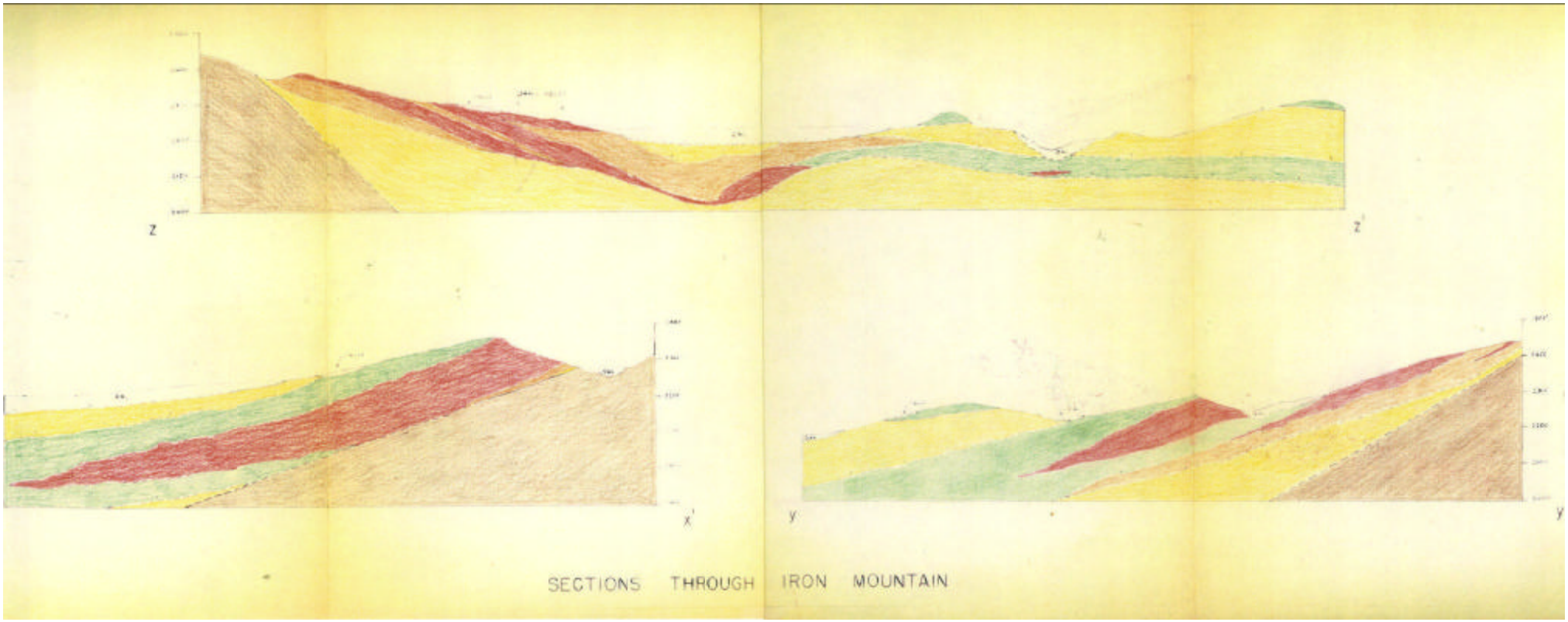

SECTIONS THROUGH IRON MOUNTAIN

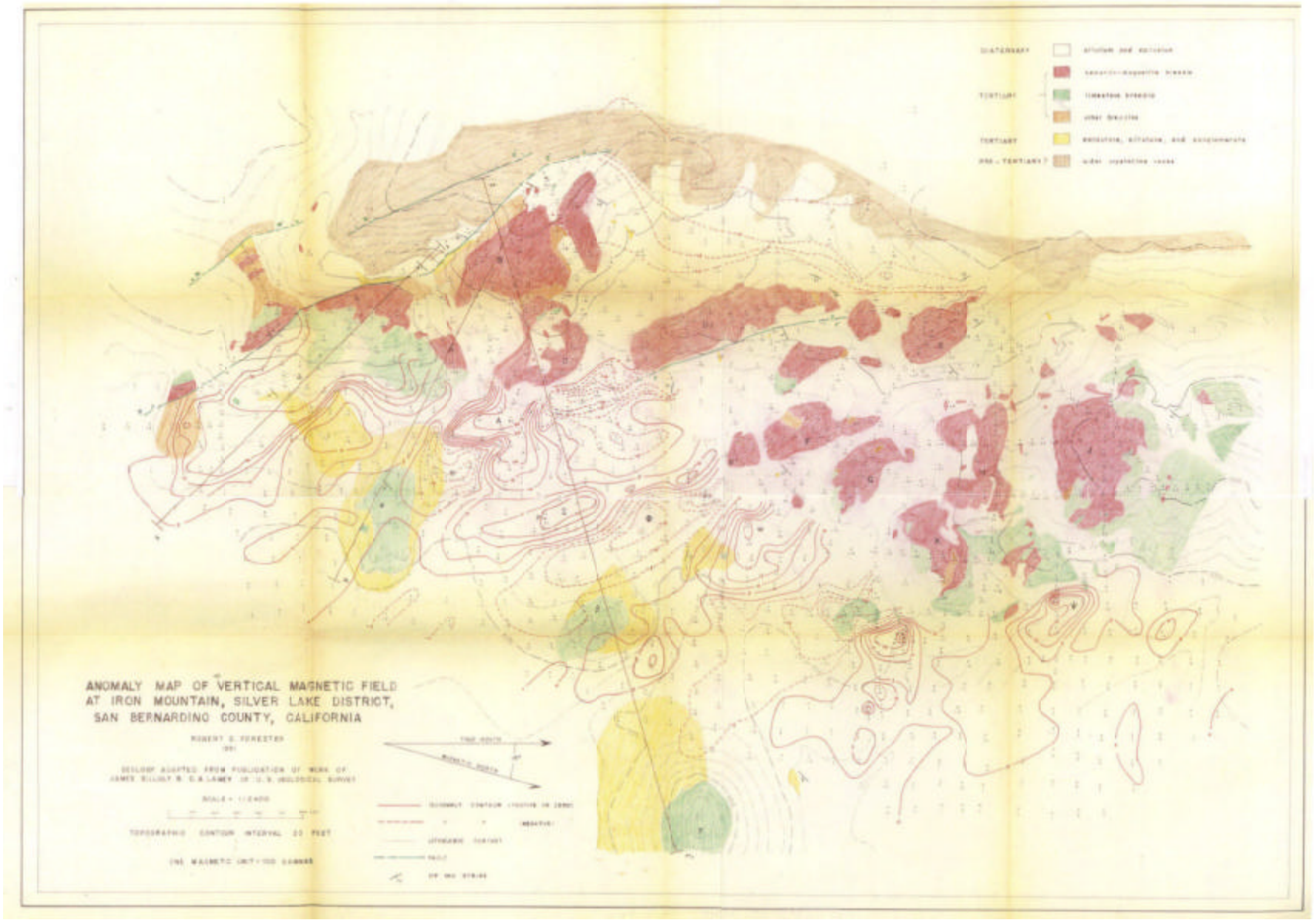
ANOMALY MAP OF VERTICAL MAGNETIC FIELD
AT IRON MOUNTAIN, SILVER LAKE DISTRICT,
SAN BERNARDINO COUNTY, CALIFORNIA